The Origin of Rhyolitic Magmas at Krafla Central Volcano (Iceland)

Shane M. Rooyakkers [1]*, John Stix[1], Kim Berlo[1], Maurizio Petrelli[2], Rachel L. Hampton[3], Simon J. Barker[4] and Daniele Morgavi[2]

[1]Department of Earth & Planetary Sciences, Mcgill University, Montreal, Québec H3A 0E8, Canada; [2]Dipartimento di Fisica e Geologia, Universitá Degli Studi di Perugia, Perugia 06123, Italy; [3]Department of Earth Sciences, 1272 University of Oregon, Eugene, Oregon, OR 97403, USA; [4]School of Geography, Environment and Earth Sciences, Victoria University of Wellington, Wellington 6012, New Zealand

*Corresponding author. National Isotope Centre, GNS Science, 30 Gracefield Rd, Lower Hutt 5040, New Zealand. Telephone: +64 4 570 1444. Fax: +64 4 570 4600. E-mail: shane.rooyakkers@mail.mcgill.ca

ABSTRACT

We present a detailed petrologic study of rhyolites from seven eruptions spanning the full ($\sim$190 ky) history of rhyolitic volcanism at Krafla volcano, northeast Iceland. The eruptions vary widely in size and style, but all rhyolites are crystal-poor (<6 modal%: plagioclase + augite ± pigeonite ± orthopyroxene ± titanomagnetite ± fayalite) and have similar evolved compositions (73.7–75.8 wt% normalized whole-rock SiO_2) and trace element patterns. Macrocryst rim compositions from each eruption cluster within a narrow range and are appropriate for equilibrium with their carrier melt. Crystal cores and interiors display complex growth patterns and commonly host resorption surfaces, but compositional variations are slight (e.g. typically <10 mol% An for plagioclase, Mg# <10 for pyroxene), and consistent with an overall trend of cooling and differentiation by crystal fractionation. Although most crystal core and interior compositions are broadly appropriate for equilibrium with melts similar to their host whole-rock, variable growth histories, juxtaposition of grains with distinct trace element compositions, and scatter in melt inclusion compositions indicate mixing of antecrysts from compositionally similar evolved melts and/or assimilated felsic mush or intrusions before final rim growth. Evidence for mafic recharge (e.g. coupled increases in An and Fe in plagioclase) is absent in most crystals; rhyolite storage and fractionation thus occurred largely in isolation from the underlying mafic system. Comparison of observed matrix glass compositions with published experimental work on melting of altered (meta)basalts casts doubt on previous models favouring rhyolite generation by partial melting of hydrothermally altered basalts, instead supporting recent isotopic and modelling arguments for a crystallization-driven process [Hampton, R. L. *et al.* (2021). *Journal of Volcanology and Geothermal Research* **414**, 107229]. MELTS fractional crystallization and assimilation-fractional crystallization (AFC) models at 1 kbar predict liquid major and trace element compositions similar to Krafla rhyolites after $\sim$60–70 vol% crystallization of a quartz tholeiite melt representative of the evolved crystal-poor basalts commonly erupted within Krafla caldera. We thus suggest that stalling and crystallization of these evolved basalts at shallow depth forms crystal mushes from which evolved (broadly dacitic to rhyolitic) melts are extracted. These melts ascend and mix with other compositionally similar melt bodies and/or assimilate felsic intrusive material in the uppermost crust. The Daly gap between $\sim$57 and 71 wt% SiO_2 at Krafla is consistent with preferential extraction of evolved melts from quartz tholeiite mushes in the $\sim$50–70% crystallinity window. Residual solid (cumulate) compositions predicted by MELTS are exclusively mafic, hence efficient silicic melt extraction from quartz

tholeiite mushes may also explain the apparent compositional bimodality in some Icelandic pluton-ic suites.

INTRODUCTION

Silicic rocks, predominantly rhyolites, form approximately 10% of the volcanic pile in Iceland (e.g. Walker, 1966; Jónasson, 2007) and ~5% of its historically-erupted magmas by volume (Thordarson & Larsen, 2007). This significant proportion of rhyolite in oceanic crust, where silicic rocks are usually rare, has intrigued petrologists since the 19th century (Bunsen, 1851), and much debate has focused on the origin of these rhyolites and their possible similarities with Earth's early continental crust (e.g. Martin *et al.*, 2008; Bindeman *et al.*, 2012; Carley *et al.*, 2014). Traditionally, most workers have favoured one of two endmember models for the petrogenesis of rhyolitic magmas in Iceland: (1) extensive fractional crystallization of basaltic melts (e.g. Carmichael, 1964; Macdonald *et al.*, 1990; Furman *et al.*, 1992), possibly with minor assimilation of altered wallrock and/or mixing with mafic magmas (Sigurdsson & Sparks, 1981; Macdonald *et al.*, 1987; McGarvie *et al.*, 1990; Nicholson *et al.*, 1991), or (2) partial melting of hydrated and hydrothermally altered basaltic crust (e.g. Óskarsson *et al.*, 1982, 1985; Condomines *et al.*, 1983; Thy *et al.*, 1990; Sigmarsson *et al.*, 1991, 1992; Jónasson, 1994) and/or silicic differentiates (Sigurdsson, 1977; Marsh *et al.*, 1991; Gunnarsson *et al.*, 1998). Several recent studies (Martin & Sigmarsson, 2007, 2010; Selbekk & Trønnes, 2007; Schattel *et al.*, 2014; Banik *et al.*, 2018; Carley *et al.*, 2020) have attempted to reconcile these differences using the concept that the local tectonic setting determines the dominant petrogenetic process. In this conceptual model, low $\delta^{18}O$ tholeiitic rhyolites are suggested to form in mature rift zones with high heat flow via near-solidus melting of altered crust (and possible subsequent crystal fractionation). In contrast, transitional-alkaline to alkaline rhyolites with normal to only slightly low $\delta^{18}O$ occur in immature rifts or off-rift settings, and predominantly form by fractional crystallization in thicker, cooler and stronger crust with less input of crustal melt. While these ideas have gone some way towards resolving the controversial origin of Icelandic rhyolites, debate persists even for individual volcanic systems (e.g. Hekla: Sverrisdottir, 2007; Portnyagin *et al.*, 2012; Lucic *et al.*, 2016; Bergþórsdóttir, 2018; Geist *et al.*, 2021).

One likely reason for the controversy around the origin of Icelandic rhyolites is that petrologic studies have generally focused on whole-rock compositions, which reflect an average of the rock-forming components (i.e. minerals ± glass). Petrogenetic models have mainly compared the major and trace element and/or isotopic compositions of rhyolites and co-existing basaltic to intermediate suites from a single system or small group of systems, often using mass balance calculations for fractional crystallization and/or assimilation to model liquid lines of descent (e.g. O'Nions and Grönvold, 1973; Macdonald *et al.*, 1987; Nicholson *et al.*, 1991; Furman *et al.*, 1992; Hemond *et al.*, 1993; Hards *et al.*, 2000). Such models have provided important insights on the over-arching processes of rhyolite generation in Iceland. However, they overlook the fine-scale heterogeneities that may be preserved in crystal zoning patterns, melt inclusions, and/or matrix glasses, each of which may have distinct origins and/or record different processes, timescales, and physicochemical conditions during the assembly of the erupted magma (e.g. Ginibre *et al.*, 2007; Cooper, 2017).

A deeper understanding of magmatic processes can be provided by linking approaches based on whole-rock chemistries with detailed microanalytical studies of mineral populations, matrix glasses, and/or melt inclusions in erupted products (e.g. Jerram *et al.*, 2018). Although phenocryst compositions are commonly reported in petrologic studies of Icelandic rhyolites, few researchers have examined these crystal cargoes and their zoning patterns in detail (e.g. Gunnarsson *et al.*, 1998; Weber & Castro, 2017). Recent studies have revealed a marked diversity in age, trace element, and isotopic compositions of the zircon cargoes in Icelandic rhyolites or felsic xenoliths from a single eruption, suggesting that these magmas comprise a mixture of melts and crystals derived from chemically and isotopically distinct sources (Carley *et al.*, 2011; Bindeman *et al.*, 2012; Gurenko *et al.*, 2015; Banik *et al.*, 2018). However, these data are limited to a handful of eruptions from a small number of volcanic systems. Similarly, relatively few studies have investigated the primary volatile contents of Icelandic rhyolites, but available data indicate widely variable magmatic H_2O contents (Elders *et al.*, 2011; Portnyagin *et al.*, 2012; Owen *et al.*, 2013a, 2013b; Zierenberg *et al.*, 2013; Schattel *et al.*, 2014; Lucic *et al.*, 2016). Further detailed microanalytical studies of Icelandic rhyolites are needed to reconcile the controversies surrounding their origin, and provide a more complete understanding of how these magmas are assembled, stored, and primed for eruption.

The Krafla volcanic system in northeast Iceland presents an excellent opportunity to study the origin and dynamics of rhyolitic magmatism in a mature rift zone setting. Recent accidental encounters with shallow rhyolitic magma (~2–2.5 km) at two sites beneath the

caldera during geothermal drilling projects (Mortensen et al., 2010; Elders et al., 2011; Zierenberg et al., 2013) confirm that the rhyolitic system remains active today, and offer a unique opportunity to study rhyolitic magma *in situ* (a goal of the Krafla Magma Testbed project; Eichelberger, 2019). Studies of previously erupted Krafla rhyolites offer a useful context with which to understand the present-day system and its active rhyolitic magma body (or bodies), as well as the long-term evolution of the volcano and the origin of silicic magmas in primitive crust. Towards these objectives, we conducted detailed petrologic studies on the products of seven eruptions spanning the full ca. 190-ky history of rhyolitic volcanism at Krafla. We present a large petrologic dataset, including new whole-rock analyses and detailed microanalysis of minerals, matrix glasses, and melt inclusions. In this paper, we consider: (1) microanalytical perspectives on the generation and assembly of Krafla's rhyolitic magmas, and (2) insights on the petrogenesis of Krafla rhyolites from major and trace element modelling and comparison with published experimental studies on melting of altered basalts and metabasalts. Comparisons between the different rhyolite units, their storage conditions, and the dynamics and evolution of Krafla's silicic system through time will be considered in a subsequent paper (Rooyakkers et al., in prep.).

GEOLOGICAL BACKGROUND AND PREVIOUS WORK

Krafla volcanic system

Krafla is one of five en-echelon volcanic systems located in the Northern Volcanic Zone of Iceland, a segment of the axial rift zone associated with the divergent Eurasian-North American plate boundary (Sæmundsson, 1979). The system comprises the Krafla central volcano, a broad shield of $\sim$25 km diameter with an $\sim$8 $\times$ 10 km caldera at its centre, and a 100 km-long, 5–8 km-wide fissure swarm that transects the central volcano from northeast to southwest (Fig. 1; Sæmundsson, 1991; Hjartardóttir et al., 2012). Volcanism and geothermal activity are mainly concentrated in and around the caldera (e.g. Árnason, 2020), which is thought to have largely formed during a major ignimbrite eruption at ca. 110 ka (Calderone et al., 1990; Rooyakkers et al., 2020; eruption age from Sæmundsson & Pringle, 2000).

The Krafla system has been active since at least 300 ka (Sæmundsson, 1991). Post-glacial activity has been dominated by basaltic fissure eruptions within and near the caldera, and along the fissure swarm to the south near Námafjall (Thorarinsson, 1979; Sæmundsson, 1991). Interplay between regional tectonics and volcanism has characterized recent activity, with long (ca. 300–1000 year) periods of tectonic and volcanic quiescence interrupted by short (<10 year) rifting events and accompanying eruptions (Hjartardóttir et al., 2016), most recently in the 1975–1984 Krafla Fires episode (e.g. Hollingsworth et al., 2012). A zone of shear-wave attenuation at $\sim$3–7 km depth in the central caldera region is inferred to reflect a shallow basaltic magma chamber (Einarsson, 1978) or network of dikes and sills (Kennedy et al., 2018). Extensive drilling associated with geothermal exploration has provided a reasonably clear outline of the subsurface geology in the central caldera region. Basaltic lavas and hyaloclastites dominate the upper $\sim$1–2 km and are underlain by an intrusive complex of basaltic dikes and gabbroic rocks, with sporadic intermediate and felsic intrusions (Ármannsson et al., 1987; Weisenberger et al., 2015).

Erupted products at Krafla are compositionally bimodal; basaltic lavas and subglacial hyaloclastites are dominant (>90% by volume), while subordinate rhyolite has erupted in and around the caldera (Nicholson et al., 1991; Sæmundsson, 1991; Jónasson, 1994). Like most rhyolites in Iceland's axial rift zone, all Krafla rhyolites have low $\delta^{18}O$ compositions; whole-rock and groundmass values are +1.0 to +3.3‰ and +2.2 to +3.6‰, respectively, compared with typical mid-ocean ridge basalt (MORB) values of +5.5 to +5.9 (Nicholson et al., 1991; Eiler, 2001; Pope et al., 2013; Hampton et al., 2021). Intermediate products are rare, and those erupted within the caldera show evidence for a hybrid origin by mixing of basalt and rhyolite in the form of mafic enclaves or streaky mingling textures (Jónasson, 1994; Rooyakkers et al., 2020). Excluding these hybrid rocks, the central volcano displays a clear Daly gap between $\sim$57 and 71 wt% SiO_2 (Jónasson, 1994).

Rhyolitic magmatism and volcanism at Krafla

Eight eruptions involving rhyolitic magma (hereafter 'units') are known from the Krafla system (summarized in Table 1; locations marked on Fig. 1). For convenience, Jónasson (1994) grouped these events into three phases of activity: (1) extrusion of a small unnamed dome (hereafter 'oldest rhyolite') at the southern edge of the Hágöng plateau, followed by the mixed basalt-rhyolite Halarauður eruption associated with major caldera collapse; (2) subglacial emplacement of the ridges Jörundur, Hlíðarfjall, and Gæsafjallarani (hereafter the 'extra-caldera ridges') around the margins of the caldera during the last glacial, possibly associated with intrusion of a ring-dike; and (3) small-volume intra-caldera eruptions, including emplacement of the Hrafntinnuhryggur ridge late in the last glacial period, and two post-glacial eruptions: the ca. 9000 BP Hveragil tephra and the 1724 CE Víti pumice. The latter occurred during the opening phase of the Mývatn Fires volcanotectonic episode and formed the small maar crater Víti (Grönvold, 1984; Sæmundsson, 1991). Products of the Víti eruption consist mainly of altered country rock, but small volumes of juvenile rhyolitic pumice and basaltic scoria were also ejected along with partially melted silicic intrusive xenoliths (Sigurdsson, 1968; Grönvold, 1984).

Molten rhyolite has been encountered twice at Krafla in recent drilling projects. In 2008, quenched glass ranging in composition from dacite to high-silica rhyolite was identified in cuttings from the bottom of well KJ-39 ($\sim$2.6 km total vertical depth) in the central region of the
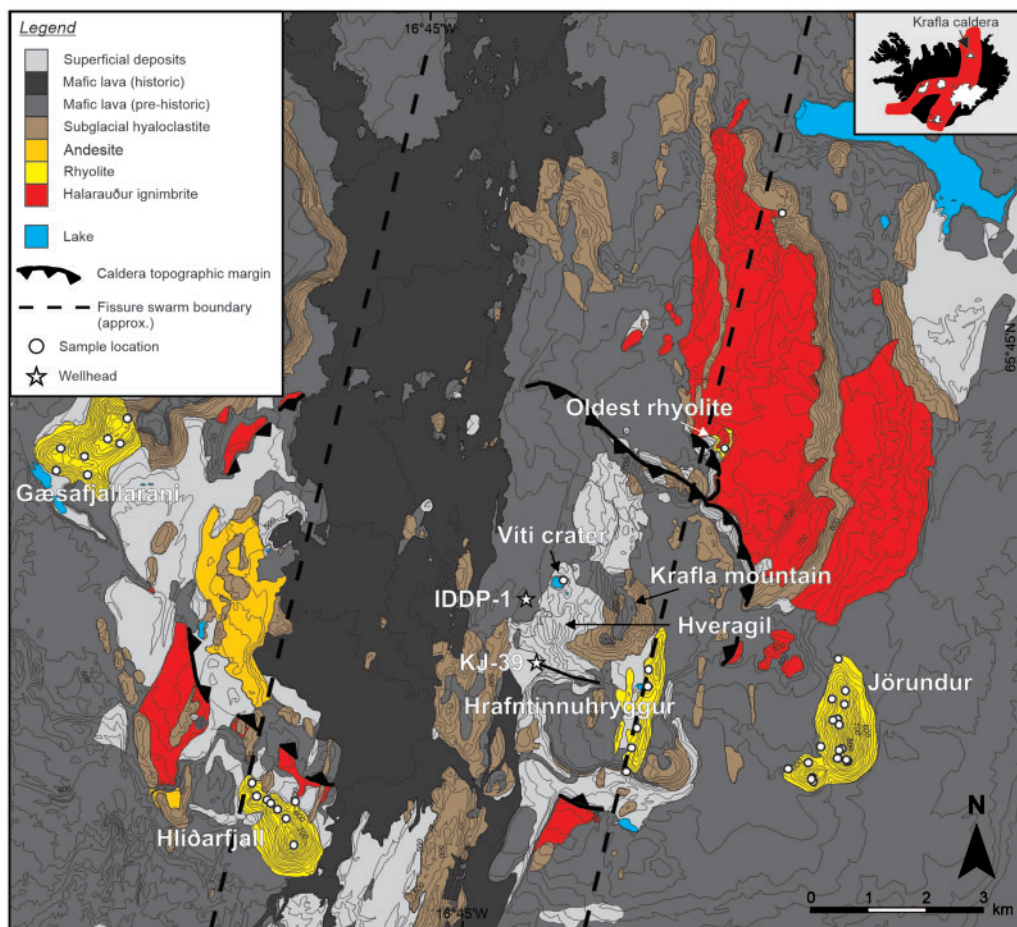
Fig. 1. Simplified geological map of the Krafla caldera and surroundings, adapted from Sæmundsson *et al.* (2012). Sampling locations for whole-rock XRF analyses are marked, as well as the IDDP-1 and KJ-39 boreholes where rhyolitic magma or melt bodies were recently intercepted. The tail extending from the KJ-39 wellhead shows the path of the slanted well. IDDP-1 was drilled vertically.

caldera, indicating that a silicic magma body or zone of partial melt had been pierced during drilling (Fig. 1) (Mortensen *et al.*, 2010). The following year, a high-silica rhyolite magma body was unexpectedly intercepted at ~2.1-km deep in the IDDP-1 well (Elders *et al.*, 2011; Zierenberg *et al.*, 2013; Schiffman *et al.*, 2014). Published bulk, mineral, and glass compositions of the IDDP-1 magma closely resemble those from the 1724 Víti rhyolite, indicating a common source (Rooyakkers *et al.*, 2021).

METHODS

Rhyolite samples were collected from seven of the eight erupted units (all except the 9 ka Hveragil tephra) during field campaigns in 2015–2017 (locations on Fig. 1; GPS coordinates are in the Supplementary Data files; Supplementary Data are available for downloading at http://www.petrology.oupjournals.org). We sampled fresh obsidian and/or microcrystalline rhyolite from subglacially erupted lava lobes across each of the extra-caldera ridges (Jörundur, Hlíðarfjall and Gæsafjallarani) and the intra-caldera ridge Hrafntinnuhryggur, as well as occasional large pumice clasts from Jörundur and

Hlíðarfjall. Widely spaced outcrops (Fig. 1) were sampled to assess any chemical variability across each ridge and to ensure representative sampling. Exposures of the oldest rhyolite are scarce and altered, so only a single, slightly altered microcrystalline sample was collected from this unit. Víti samples comprise fresh pumice collected inside Víti crater. The Halarauður ignimbrite spans a continuous compositional range from basalt to rhyolite and shows textural evidence for magma mixing (Calderone *et al.*, 1990; Rooyakkers *et al.*, 2020). A detailed petrologic study of all Halarauður products will be presented elsewhere (Rooyakkers *et al.*, in prep.). For comparison with the other rhyolites, we here report the bulk composition of a pumice sample collected from the basal ignimbrite unit (H1 of Rooyakkers *et al.*, 2020), which is the most evolved Halarauður sample that we analysed and is considered to represent the rhyolitic mixing endmember.

Powdered whole-rock samples were analysed for major element contents by X-ray fluorescence spectroscopy (XRF) in New Zealand at the University of Auckland or the University of Waikato. A subset of 22 samples, selected to cover the full range of major element compositions, were analysed for trace element contents by

Table 1: Overview of Krafla rhyolite units

Unit	Age	Volume (km^3)	Description
Oldest rhyolite (unnamed)	ca. 190 ka[a]	<0.05[d]	Small dome NE of the present caldera margin, poorly exposed beneath Halarauður ignimbrite
Halarauður ignimbrite	110–115 ka[a]	Total 7 ± 6[e] (∼50% rhyolite, ∼50% basalt)[f]	Ignimbrite sheet related to caldera collapse event. Mixed basalt-rhyolite eruption. Rhyolite pumice common in basal deposits, later-erupted material mostly hybrid compositions[e,f]
Jörundur	88.7 ± 9.9 ka[b]	∼0.15	Subglacially erupted ridge, rising ∼250–300 m above surrounds[d,h]
Gæsafjallarani	85.5 ± 9.4 ka[b]	∼0.15	Subglacially erupted ridge, rising ∼250–300 m above surrounds[d,h]
Hlíðarfjall	83.3 ± 9.2 ka[b]	0.14[g]	Subglacially erupted ridge, rising ∼250–300 m above surrounds[d,h]
Hrafntinnuhryggur	ca. 24 ka[a]	0.02[g]	Dike erupted beneath thin ice, lobes of micro-crystalline rhyolite and obsidian[i]
Hveragil tephra	ca. 9000 BP[c]	n.q.	Small explosive mixed basalt-rhyolite eruption from the Víti area, dispersed pumice across the central and southern caldera region[c,d]
Víti	1724 CE[c]	n.q.	Rhyolitic pumice co-erupted with small volumes of basaltic scoria and partially melted grano-phyric xenoliths in a phreatomagmatic event during the opening phase of the Mývatn Fires, forming the maar crater Víti[c,d,j]

[a]Sæmundsson & Pringle (2000).
[b]Hampton *et al.* (2021).
[c]Sæmundsson (1991).
[d]Jónasson (1994).
[e]Rooyakkers *et al.* (2020).
[f]Rooyakkers (2020).
[g]Agustsdottir *et al.* (2010).
[h]McGarvie (2009).
[i]Tuffen & Castro (2009).
[j]Rooyakkers *et al.* (2021).
n.q. = not quantified, but estimated as ≪0.01 km^3 based on published accounts of dispersal.

inductively-coupled plasma–mass spectrometry (ICP–MS) by Actlabs (Ancaster, Canada). Mineral and glass major- and minor-element compositions were determined by electron probe microanalysis (EPMA) at McGill University (Montreal, Canada), and trace element contents were determined by laser-ablation ICP–MS at the University of Perugia (Italy). Analytical methods and data quality are outlined in the Supplementary Data Methods file. Analyses of standard reference materials used to assess analytical precision and accuracy are included with all data in Supplementary Data Excel spreadsheets.

RESULTS

Petrography

For the purposes of this paper, crystals larger than the groundmass are defined as 'macrocrysts' (>0.05 mm for titanomagnetite, and >0.1 mm for other phases). All Krafla rhyolites studied here are crystal-poor, with <6 modal% macrocrysts hosted in a glassy to devitrified spherulitic groundmass. Hrafntinnuhryggur samples are aphyric. Sparse plagioclase and augite crystals in Halarauður rhyolite pumice were mainly inherited during mixing with basaltic magmas, so will be considered elsewhere.

Plagioclase is the dominant macrocryst in all phyric samples, comprising up to 5 modal% (Table 2). In all samples it occurs as euhedral, tabular to prismatic crystals reaching up to ∼4 mm in the extra-caldera rhyolites and ∼2 mm in Víti pumices, as well as occasional glomerocrysts (±pyroxene, fayalite, and/or titanomagnetite). Complex optical zoning and inclusions of melt, zircon (extra-caldera ridges only), and apatite are common. Green, euhedral to subhedral (rarely skeletal) augite up to ∼1 mm is a ubiquitous minor phase, comprising up to 0.6 modal% (Table 2). Fine exsolution lamellae of pigeonite are common in Víti augite macrocrysts, but rare in those from the extra-caldera ridges. Around 50% of augites occur as glomerocrysts with plagioclase and/or titanomagnetite, in some cases with minor interstitial glass. Small (<50 μm) inclusions of glass, apatite and/or Fe-Ti oxides are common. Pigeonite and orthopyroxene are minor phases (together <0.1 modal%) in all but the oldest rhyolite. For Víti, both phases occur as rare, discrete euhedral to subhedral grains up to ∼0.5 mm, often with augite exsolution lamellae, but are more common in composite grains where they overgrow or are overgrown by augite. In the three extra-caldera ridges, pigeonite and orthopyroxene occur only as rare cores mantled by augite. Euhedral to subhedral titanomagnetite up to ∼0.3 mm (typically <0.1 mm) occurs in all units (up to 0.3 modal%), both as inclusions in plagioclase and mafic minerals and as a discrete phase. Fayalite was identified in Jörundur and Gæsafjallarani samples only,

Table 2: Representative modes for Krafla rhyolites

Sample number	Unit	Plagioclase	Augite	Pigeonite + Orthopyroxene	Titanomagnetite	Fayalite	Granophyric clots	Zircon	Apatite
KR-6-a	Víti	4.5	–	<0.1	0.2	–	0.5	–	Trace
KR-6-l	Víti	1.9	–	<0.1	0.1	–	0.5	–	Trace
KR-153-e	Víti	2.7	0.3	<0.1	0.0	–	–	–	Trace
KR-40	Hlíðarfjall	1.8	0.2	<0.1	<0.1	–	–	Trace	Trace
KR-123	Jörundur	4.3	0.4	0.1	0.2	–	–	Trace	Trace
KR-128	Jörundur	2.7	0.2	0.0	0.2	0.1	–	Trace	Trace
KR-129	Jörundur	4.1	0.3	0.1	0.2	0.4	–	Trace	Trace
KR-147	Gæsafjallarani	4.2	0.6	<0.1	0.3	0.2	–	Trace	Trace
KR-106	Oldest rhyolite	1.1	0.1	–	0.1	–	–	–	Trace

Modal compositions (in %, normalized void-free) determined from image analysis of high-resolution scans or BSE maps of polished thin sections using ImageJ (https://imagej.nih.gov).

Table 3: Representative whole-rock compositions for Krafla rhyolites

| Sample	KR-24	KR-179	KR-112	KR-169	KR- 128	KR- 106	KR- 14-n
Unit	Gæsafjallarani	Halarauður	Hlíðarfjall	Hrafntinnuhryggur	Jörundur	Oldest Rhyolite	Víti
Type	Lava	Pumice	Lava	Obsidian	Lava	Lava	Pumice
Major oxides (wt%)							
SiO_2	74.12	74.57	75.63	74.83	74.50	73.97	73.94
Al_2O_3	12.12	12.37	12.14	12.21	12.10	12.53	12.49
TiO_2	0.34	0.29	0.24	0.24	0.31	0.41	0.38
MnO	0.10	0.09	0.07	0.10	0.09	0.08	0.08
$Fe_2O_3^T$	4.36	3.86	3.30	3.73	4.22	4.40	4.06
MgO	0.18	0.22	0.06	0.12	0.15	0.33	0.30
CaO	1.94	1.86	1.65	1.68	1.79	1.57	1.90
Na_2O	4.16	4.05	4.15	4.37	4.16	4.06	3.96
K_2O	2.62	2.64	2.75	2.70	2.63	2.58	2.82
P_2O_5	0.05	0.04	0.02	0.04	0.04	0.07	0.07
Total	100	100	100	100	100	100	100
LOI	1.71	0.90	1.69	0.18	0.64	2.10	0.73
Raw analytical total	99.46	97.87	99.38	100.12	99.41	99.46	98.42
Mg#	9	13	4	7	8	15	16
An#	11	11	10	10	10	10	11
Trace elements (ppm)							
V	BDL	BDL	BDL	BDL	BDL	5	5
Co	BDL	BDL	BDL	1	1	2	2
Cu	10	10	20	10	10	BDL	20
Zn	110	100	110	120	100	120	60
Ga	21	20	20	23	20	22	18
Rb	68	59	69	62	67	69	68
Sr	95	85	91	97	90	118	76
Y	96	81.4	97.2	95	94.1	68.4	70.5
Zr	523	433	480	523	572	607	455
Nb	46.1	38.9	46.6	52.7	48	57.3	33.7
Cs	0.8	0.6	0.8	0.7	0.8	0.5	0.8
Ba	527	483	556	566	531	546	515
La	50.9	45.5	52.7	57.6	50.7	50.9	42.7
Ce	110	100	113	124	108	101	90.3
Pr	13.5	12.3	13.8	15.1	13.4	13.9	10.7
Nd	55.7	50.9	55.8	62.1	56.5	57	41.9
Sm	13.5	12.5	13.6	14.5	13.6	13.2	10.3
Eu	2.78	2.48	2.67	2.81	2.64	3.03	2.02
Gd	14.5	12.8	14.9	15.5	14.4	12.8	10.8
Tb	2.47	2.17	2.54	2.58	2.42	2.04	1.82
Dy	15.6	13.8	16.1	16.3	15.5	12.8	11.9
Ho	3.28	2.88	3.39	3.43	3.30	2.51	2.49
Er	9.76	8.77	10.10	10.10	9.87	7.44	7.32
Tm	1.48	1.27	1.54	1.56	1.48	1.11	1.15
Yb	10.00	8.90	10.30	9.92	10.10	7.62	7.66
Lu	1.53	1.34	1.57	1.54	1.54	1.17	1.20
Hf	12.2	11.1	11.7	12.5	13.2	13.6	11.3
Ta	BDL	2.79	3.32	3.75	3.33	4.03	2.67
Tl	0.14	0.12	0.23	0.11	0.13	0.12	0.69
Pb	BDL	BDL	7	BDL	BDL	BDL	6
Th	6.96	6.51	7.23	7.34	7.06	6.42	7.42
U	2.15	1.97	2.22	2.29	2.15	1.86	2.22

BDL = below detection limit. Mg# Calculated assuming Fe3+/ΣFe = 0.2. An# calculated after Waters & Lange (2015).

as anhedral crystals up to ~1 mm. Apatite is a common accessory phase, occurring both as discrete grains and as inclusions in other minerals. Accessory zircon was also identified, both as discrete grains and inclusions in macrocrysts in the extra-caldera ridge rhyolites. Zircon was not observed in any of the other units studied, either as inclusions or discrete grains, and traditional extraction methods applied by Hampton *et al.* (2021) also failed to yield zircons for these units. Occasional irregular clots of granophyric material (intergrown quartz and K-feldspar)

up to ~0.5 mm occur in Víti pumices; quartz is otherwise absent.

Whole-rock chemistry

Representative whole-rock analyses are shown in Table 3. Krafla rhyolites are metaluminous, with 2.5–2.9 wt% K_2O and 73.7–75.8 wt% SiO_2 (normalized anhydrous). Major element compositions from each unit define discrete compositional fields with minor scatter (Fig. 2), as noted by Jónasson (1994). Hlíðarfjall samples are the
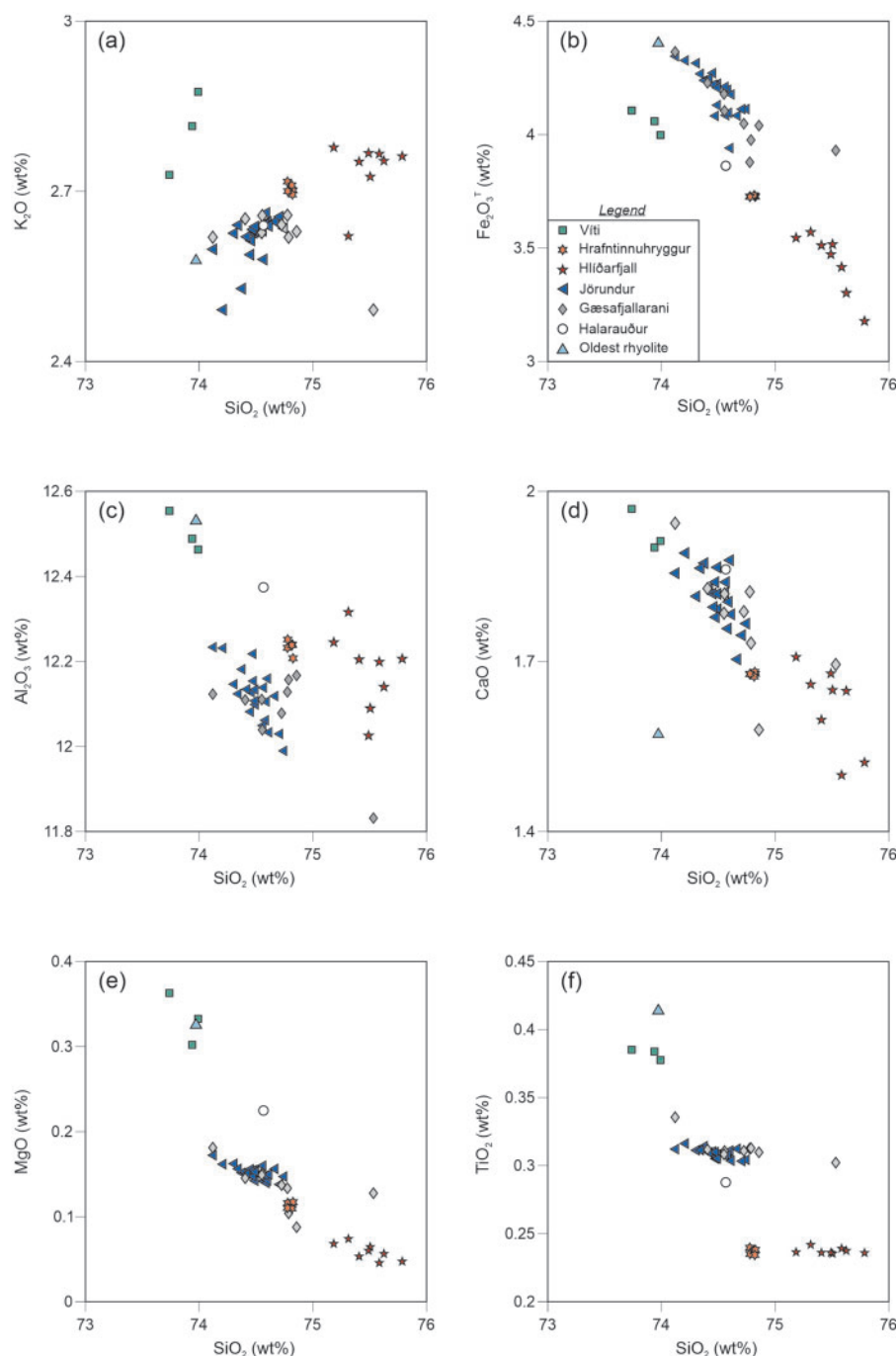
Fig. 2. Selected whole-rock major element plots (analysed by XRF). All data are normalized volatile-free with total iron as Fe_2O_3. Estimated 2σ analytical uncertainties are smaller than the symbols.

most evolved of the suite, with the lowest $Fe_2O_3^T$, MnO and MgO, and highest SiO_2 contents (excluding KR-148 from Gæsafjallarani, which has anomalously high SiO_2 and low Na_2O and Al_2O_3; Fig. 2). Víti pumices and the oldest rhyolite have the least evolved compositions (e.g. lower SiO_2 and higher TiO_2, Al_2O_3, MgO, and $Fe_2O_3^T$ than the rest of the suite). Minor compositional scatter within each unit is readily accounted for by small differences in crystal content and phase proportions. For example, least-squares mass balance calculations using representative phase compositions (see below) indicate that the most evolved Jörundur composition (KR-142) can be derived from the least evolved Jörundur composition (KR-96) by removal of 2.7 wt% crystals (80% plagioclase, 4% titanomagnetite, and 16% fayalite; calculations in Supplementary Data Table S1). Minor variations in phase abundance and proportions are supported by the modal data in Table 2.

All units show similar trace element patterns, with large negative Sr, P, and Ti anomalies, and small negative Nb and positive Zr anomalies (Fig. 3a). Chondrite-normalized rare earth element (REE) patterns for all units show LREE enrichment ($[La/Yb]_N = 3.28–4.54$), steep LREE-MREE trends ($[La/Sm]_N = 2.27–2.74$), negative Eu anomalies ($Eu/Eu^* = 0.56–0.71$), and relatively flat MREE-HREE trends ($[Dy/Lu]_N = 0.95–1.09$) (Fig. 3b). The overall shapes of the REE patterns are essentially indistinguishable for all but the oldest rhyolite, which has notably higher LREE/HREE, a steeper MREE trend from Gd to Ho, and a shallower Eu anomaly.

Mineral chemistry
Plagioclase
Plagioclase core compositions in Krafla rhyolites range from An_{27} to An_{62}, mainly clustering between $\sim An_{35–50}$, while rims range from An_{28} to An_{50} (Fig. 4a). Cores from individual units span ranges of $\sim$20–25 mol% An, while rims vary by $\sim$15 mol% An (5 mol% for the oldest rhyolite) (Fig. 4a).

Net (i.e. core to rim) zoning is subtle, rarely exceeding 10 mol% An and 0.2 wt% FeO* (Fig. 4). All erupted units contain both normal- and reverse-zoned plagioclase, although normal zoning is more common. Many crystals show no net major or trace element zoning within 2σ analytical uncertainty; notable exceptions are minor rim enrichments in Sr relative to cores (up to 110 ppm, usually <50 ppm) for some Hlíðarfjall and Víti crystals (70 and 57%, respectively), as well as relative rim enrichments in Eu and depletions in Mg for Víti crystals with the most calcic cores (not shown).

Despite only minor core-rim zoning, the internal zoning patterns of individual crystals are often complex. We recognize eight texturally distinct zoning types, summarized in Table 4. All rhyolites host at least seven of these types (Fig. 5). A minimum of 25% of crystals from each unit contain at least one internal resorption surface (dark resorbed core, multiple resorption, patchy, and some bright core types; Fig. 5). Internal resorption textures are particularly prominent in Víti crystals ($\sim$75%). However, intra-crystal chemical variations in all units are usually minor. Most resorption surfaces are overgrown by more calcic compositions (brighter in back-scattered electron [BSE] images), but compositional differences across them are rarely >10 mol% An (often <5 mol%), and only 12% show a coupled increase in An and FeO*. Total intra-crystal An zoning is rarely >10 mol% and never >20 mol%. Intra-crystal FeO* variations reach a maximum of 0.36 wt% but exceed the 2σ analytical uncertainty (0.12 wt%) in only 15% of crystals. Minor intra-crystal Sr variations ($\sim$30–60 ppm) are common (40% of crystals), but only 6% of crystals show variations comparable to the 100–150 ppm range of rim compositions present in each unit. Similarly, Ba zonation is <50 ppm in half of the crystals analysed, while variations of 100–200 ppm, comparable to the total range of rim Ba contents in each unit, occur in only 14% of crystals. Hence, within each unit, inter-crystal differences in plagioclase trace element compositions outweigh those within individual crystals.
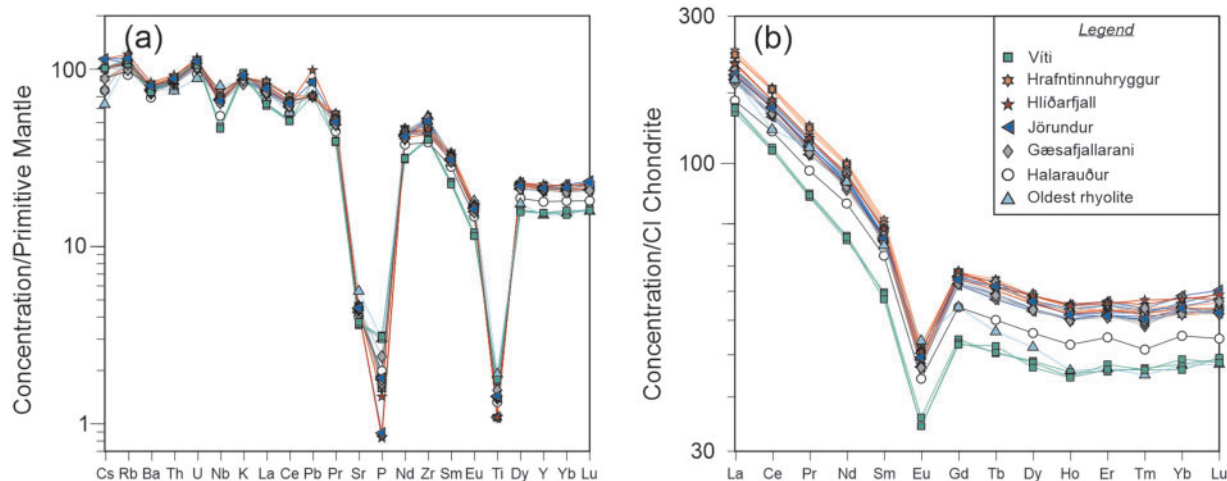
Fig. 3. Whole-rock trace element plots (analysed by ICP–MS) normalized to (a) the primitive mantle values of Sun & McDonough (1989) and (b) the chondrite values of McDonough & Sun (1995), respectively.
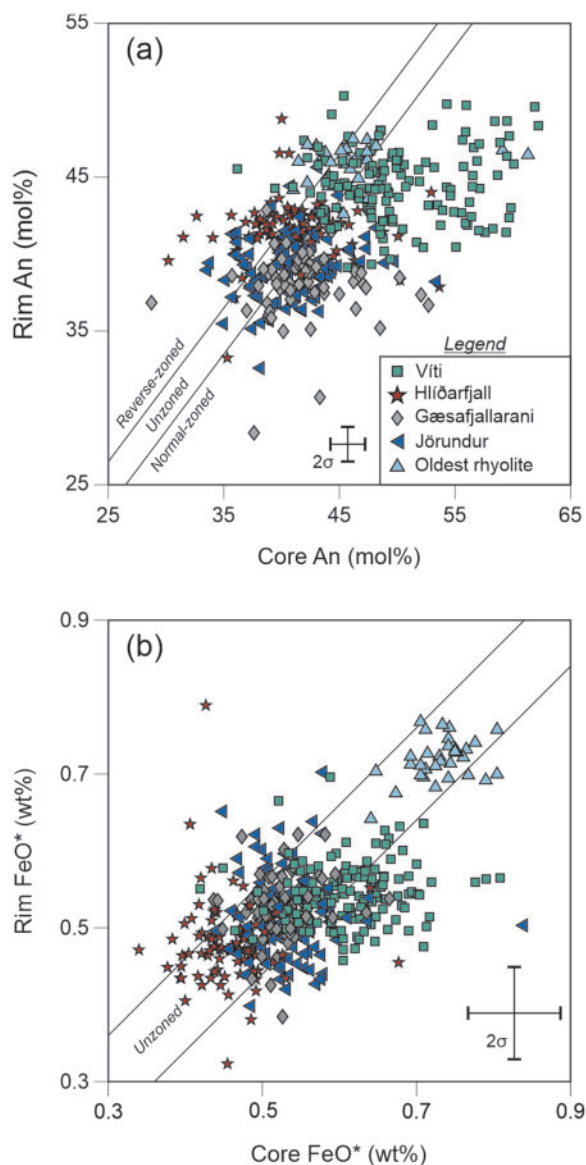
Fig. 4. Rim vs core (a) An content and (b) FeO* for plagioclase macrocrysts (analysed by EPMA). Estimated 2σ analytical uncertainties were determined from repeat analyses of NMNH 115900 plagioclase.

Pyroxene

Augite is the dominant pyroxene in both the extra-caldera ridges and Víti, occurring as a discrete phase and as overgrowths on pigeonite and orthopyroxene, as well as intergrowths with pigeonite in Víti samples. Core, interior, and rim compositions for the extra-caldera ridges mainly cluster on the Fe-rich side of the ternary, with occasional magnesian cores and interiors from Jörundur and Gæsafjallarani extending up to Mg# 72 (Fig. 6a–c). Víti core compositions are more magnesian and less clustered than the other rhyolites, with cores and interiors also reaching up to Mg# 72. Cr contents are usually below detection limit (<2–3 ppm) for the extra-caldera ridges and <10 ppm for Víti; rare high-Mg# cores and interiors from Gæsafjallarani and Víti reach up to 150 and

450 ppm, respectively, and are similarly enriched in other compatible transition metals (Co, Ni, and V; Fig. 6e).

Pigeonite is a minor phase in the Víti rhyolite. Cores and interiors range from $En_{28-43}Fs_{47-64}Wo_{8-10}$ (Mg# 31–48; Fig. 6a and b). Most Víti pigeonites are overgrown by augite, but a minority have rims of more Fe-rich pigeonite, and pigeonite rims of $En_{27-33}Fs_{59-63}Wo_{8-10}$ (Mg# 31–37) also occasionally mantle Víti augite cores (Fig. 6c). In the extra-caldera ridges, pigeonite occurs as rare cores, and/or interiors of $En_{18-39}Fs_{52-72}Wo_{8-10}$ (Mg# 20–44), mantled by augite.

Orthopyroxene is rare in Krafla rhyolites, but cores and/or interiors overgrown by either augite or pigeonite were observed in occasional grains from Hlíðarfjall ($En_{25-44}Fs_{53-73}Wo_{3-4}$; Mg# 26–46), Jörundur ($En_{49-65}Fs_{31-48}Wo_{3-4}$; Mg# 51–68), and Víti ($En_{36-64}Fs_{32-61}Wo_{3-4}$; Mg# 38–67) (Fig. 6a and b). Additionally, a single discrete subhedral grain of orthopyroxene ($En_{36-47}Fs_{50-61}Wo_{3-4}$; Mg# 38–49) was identified in hand-picked mineral separates from a crushed Víti pumice.

Like plagioclase, compositional zoning in augites from Krafla rhyolites is usually subtle. Normal core-rim zoning is common (57% of crystals), but rarely exceeds Mg# 10, while reverse zoning is scarce (13% of crystals) and limited to Mg# <5 (Fig. 6d). Intra-crystal zoning exceeds Mg# 10 in only one-third of crystals. Nonetheless, like plagioclase, internal zoning patterns in individual crystals can be complex. We recognize nine distinct zoning types, summarized in Table 5 and Fig. 7. Each unit hosts 5–7 of these types. Large-magnitude intra-crystal zoning (Mg# variations >20; 12% of crystals) occurs almost exclusively in crystals with prominent resorption surfaces (dark resorbed core and patchy types; Table 5, Fig. 7), and occasionally in Víti augites intergrown with or overgrown by pigeonite. Intra-crystal trace element variations largely mirror the major elements; decreases in Mg# usually correspond with lower V, Ni, and Co and higher Sc, Y, and REE contents, but compositional shifts are often slight (e.g. 85% of intra-crystal Co zoning is <10 ppm, 90% of V zoning is <30 ppm).

Fayalite

Fayalite (Fo_{11-17}) occurs sparsely in the Jörundur and Gæsafjallarani rhyolites (Table 2). All crystals are anhedral and unzoned, with 35–43 ppm Co and 5–9 ppm Ni.

Fe-Ti oxides

Homogeneous grains of titanomagnetite are ubiquitous in the crystal-bearing rhyolites. Occasional trellis-type grains with ilmenite lamellae also occur in some Jörundur, Gæsafjallarani, and oldest rhyolite samples. These exsolved grains are inferred to reflect oxidation-exsolution during post-eruptive cooling (Haggerty, 1991) and are not considered further. Ilmenite was otherwise not identified in thin section or grain mounts except for a single euhedral grain (Ilm_{95}) from Hlíðarfjall.

Table 4: Plagioclase zoning types

| Schematic	Zoning type	Description	Sr Zoning (ppm)	Ba Zoning (ppm)
	Unzoned	No discernible zoning	<30	<50
	Smooth normal	Gradational zoning from more calcic (BSE brighter) core to more sodic (BSE darker) rim. No reversals or sharp compositional boundaries. Intra-grain An variations usually <5–10 mol%, rarely up to 15 mol%	<30–33 (median = 28)	<50–60 (median = 51)
	Subtle oscillatory	Fine-scale concentric oscillations, most zones <20-μm thick. Adjacent zones vary by ~1–3 mol% An. Total intra-grain variations are <10 mol% An, rarely exceeding 5 mol%	<30–47 (median = 6)	<50 (median = 17)
	Prominent oscillatory	Broad concentric oscillatory zones, commonly >50–100-μm thick. Contacts between zones range from sharp to gradational. Adjacent zones vary by up to 7 mol% An. Total intra-grain variations reach up to ~20 mol% An, but rarely exceed 10 mol%	<30–104 (median = 29)	<50–169 (median = 55)
	Dark resorbed core	BSE dark, rounded/resorbed core mantled by a smooth normal or oscillatory over-growth. Cores may show minor internal normal or oscillatory zoning. Intra-grain An variations typically <5–10 mol%, occasionally up to 15–20 mol%	<30–114 (median = 38)	<50–190 (median = 47)
	Bright core	Large, homogeneous or subtly zoned BSE bright core in sharp contact with darker overgrowth. May have an oscillatory mantle. Intra-grain An variations typically ~5–10 mol%, occasionally up to ~15 mol%	<30–125 (median = 67)	55–169 (median = 105)
	Multiple resorptions	Resorbed inner core overgrown by oscillatory mantle with one or more resorption surfaces. Intra-grain An variations typically <5–10 mol%, occasionally up to 15 mol%	<30–77 (median = 60)	<50–146 (median = 69)
	Patchy	Heavily resorbed core with complex, patchy zoning. Intra-grain An variations are usually <5 mol%, occasionally up to 15 mol%	<30–158 (median = 53)	<50–99 (median = 40)

Titanomagnetite compositions from Jörundur, Gæsafjallarani, and Hlíðarfjall are tightly clustered, with ranges comparable to the 2σ analytical uncertainty for most elements [Fig. 8; Fe and totals recalculated after Carmichael (1967); mol% Usp calculated after Stormer (1983)]. Excluding one outlier (Usp_{30}), Jörundur and Gæsafjallarani compositions are indistinguishable within error (Usp_{51-61}). Hlíðarfjall extends to more Ti-rich compositions (Usp_{58-68}). Compositions for the oldest rhyolite (Usp_{45-60}) mostly fall within or near the range for Jörundur and Gæsafjallarani, but low recalculated totals (95.9–98.8 wt%) are consistent with textural evidence for minor alteration. Víti titanomagnetites range between Usp_{52-66}, excluding two outliers with $\sim Usp_{35}$.

Glass chemistry
Matrix glass
Matrix glasses from Jörundur, Hlíðarfjall, Hrafntinnuhryggur, and Víti are rhyolitic (>74.5 wt% SiO_2, normalized anhydrous). Analyses from each unit cluster within distinct compositional fields. Although the spacing between fields is less than the analytical uncertainty, mean compositions are distinct within $\pm 2\sigma_M$ (where σ_M is the standard error of the mean) (Fig. 9). Chondrite-normalized REE patterns for each unit are essentially parallel and mirror the whole-rock patterns, with steep LREE-MREE and flat MREE-HREE trends, and negative Eu anomalies (Eu/Eu* = 0.47–0.61; Fig. 10a). Due to extensive groundmass devitrification, we were unable to obtain reliable matrix glass analyses for Gæsafjallarani and the oldest rhyolite.

Melt inclusions
Melt inclusion compositions are exclusively rhyolitic (Fig. 9). For each unit, melt inclusion analyses show greater compositional spread than matrix glasses, although their average compositions are similar and most melt inclusions analyses fall within 2σ analytical error of the average matrix glass. Exceptions are two slightly more primitive augite-hosted inclusions from Víti and three plagioclase-hosted inclusions from Hlíðarfjall that extend to lower SiO_2 and higher Al_2O_3, FeO*, CaO, P_2O_5, MgO, and/or TiO_2. The three primitive Hlíðarfjall inclusions are also enriched in Zr (Fig. 10c), Hf, Sc, and Eu relative to matrix glasses and all or most other Hlíðarfjall inclusions. Trace element compositions of most other inclusions overlap almost completely with their corresponding matrix glasses for most elements; notable exceptions are a subset of inclusions from Hlíðarfjall and Jörundur and a single inclusion from Víti with shallower Eu anomalies (Eu/Eu* = 0.65–0.95; Fig. 10b), three Víti inclusions near the middle of the SiO_2 range with low REE and Y contents (Fig. 10b and c), and an additional two Víti inclusions with high Mg and/or Ti (Fig. 10d).
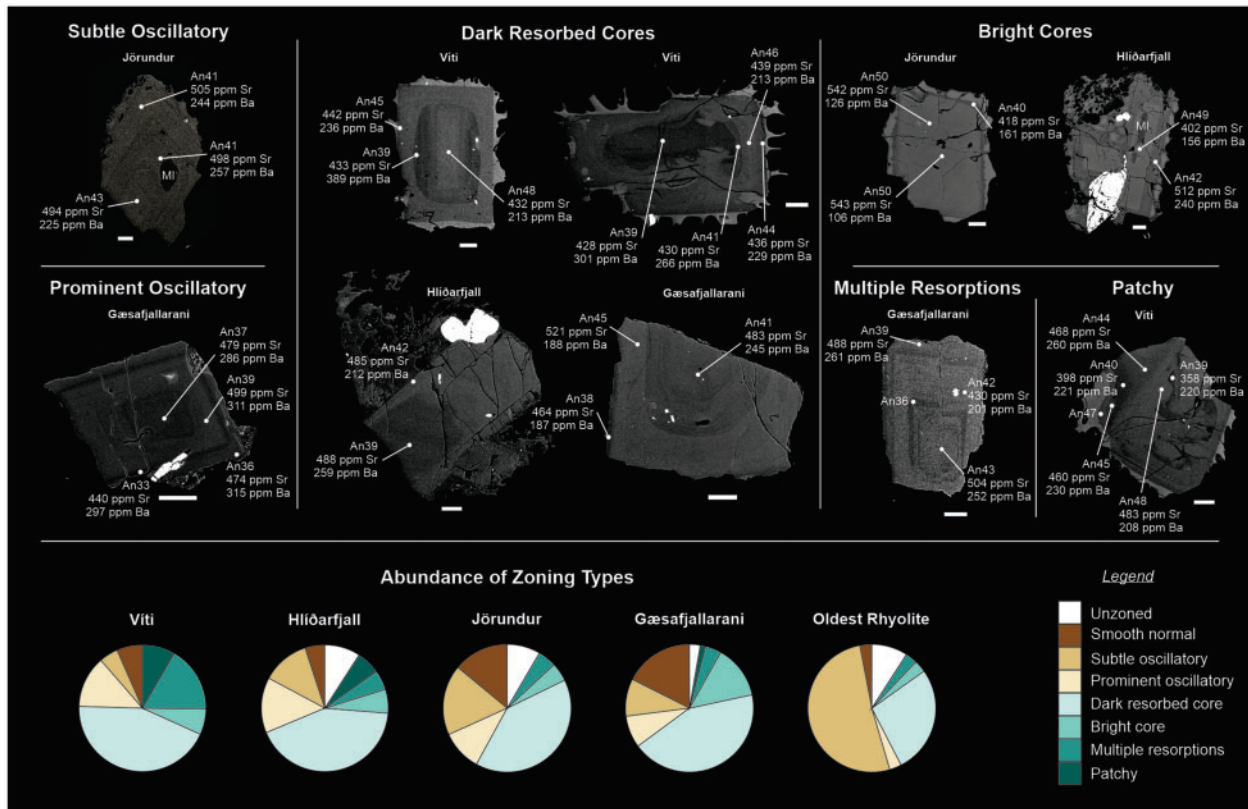
Fig. 5. Labelled back-scattered electron (BSE) images of selected plagioclase crystals, highlighting zoning types and associated variations in An, Sr, and Ba content. Pie charts show the relative proportion of each zoning type within each unit. Melt inclusions are labelled 'MI'. Scale bars are 100 μm.
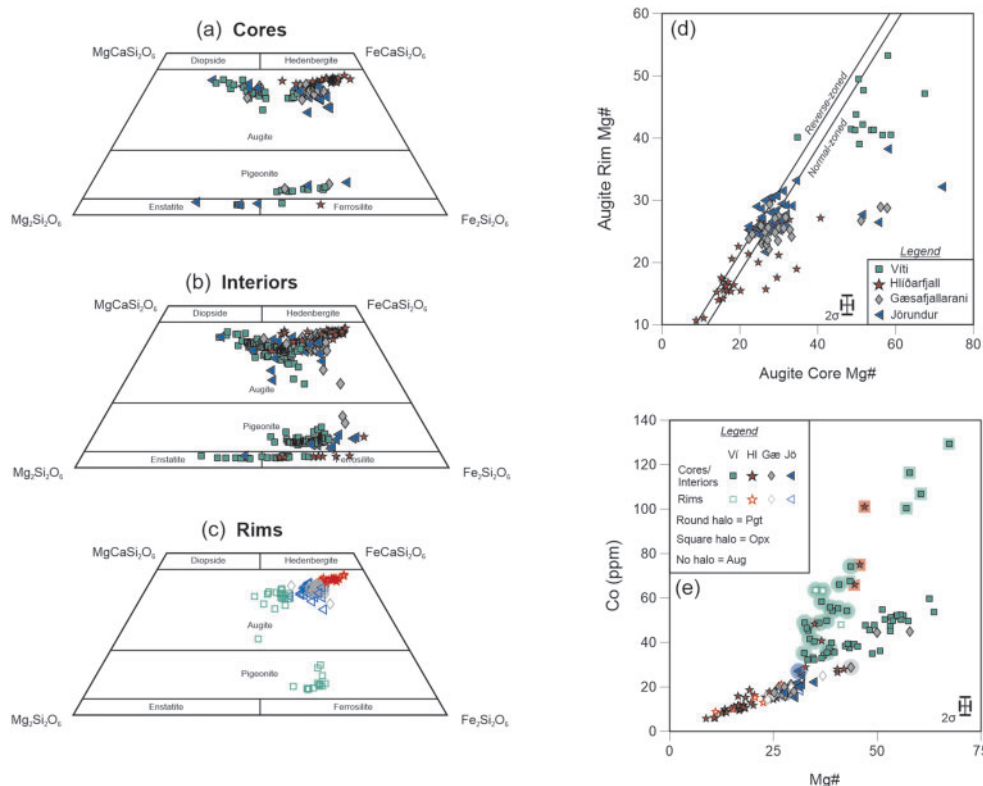
Fig. 6. Selected compositional plots for pyroxenes. Major and trace elements were determined by EPMA and LA–ICP–MS, respectively. Analytical uncertainties (2σ) were determined from replicate analyses of Taylor Diopside (EPMA) and BCR-2G glass (LA–ICP–MS) standards.

Table 5: Augite zoning types

| Schematic	Zoning type	Description
	Unzoned	No discernible zoning
	Smooth normal	Gradational normal zoning from BSE darker core to brighter rim. No reversals or sharp compositional boundaries. Inta-grain Mg# variations are usually <5–10, rarely reaching up to 25
	Smooth reverse	Gradational reverse zoning from BSE brigher core to darker rim. No reversals or sharp compositional boundaries. Intra-grain Mg# variations are <5
	Concentric	Concentric zones. Internal boundaries may show evidence for minor resorption, but growth zones do not cross-cut. Intra-grain Mg# zoning is usually <5–10 and occasionally up to 15
	Dark resorbed core	BSE dark, rounded and resorbed core mantled by a smooth normal or oscillatory overgrowth (sharp or narrow diffuse contact <50 µm). Large intra-grain Mg# variations, usually 20–30
	Patchy	Heavily resorbed core/interior with complex, patchy zoning. Intra-grain Mg# variability is usually <5–10, but can be large (maximum of 35)
	Pigeonite or orthopyroxene core	Partially resorbed core of orthopyroxene (BSE dark) or pigeonite (BSE bright), overgrown with augite. Occasionally, orthopyroxene cores are mantled by pigeonite with an augite rim. Augite overgrowths may show normal or patchy zoning, with variations in Mg# up to 20
	Pigeonite overgrowth	High-Mg# (50–70) augite core overgrown with less magnesian, normally zoned pigeonite (Mg#30–45). Cores range from faceted to resorbed and may show complex internal zoning
	Augite-pigeonite intergrowths	Intergrowths of pigeonite and augite, often with complex boundaries. Both pigeonite and augite may host thin (<1 µm) exsolution lamellae of the other phase. High-Mg# orthopyroxene occasionally occurs as cores within pigeonite. Intra-grain Mg# variations in augite range from <10 up to 25; pigeonite Mg# varies by <10
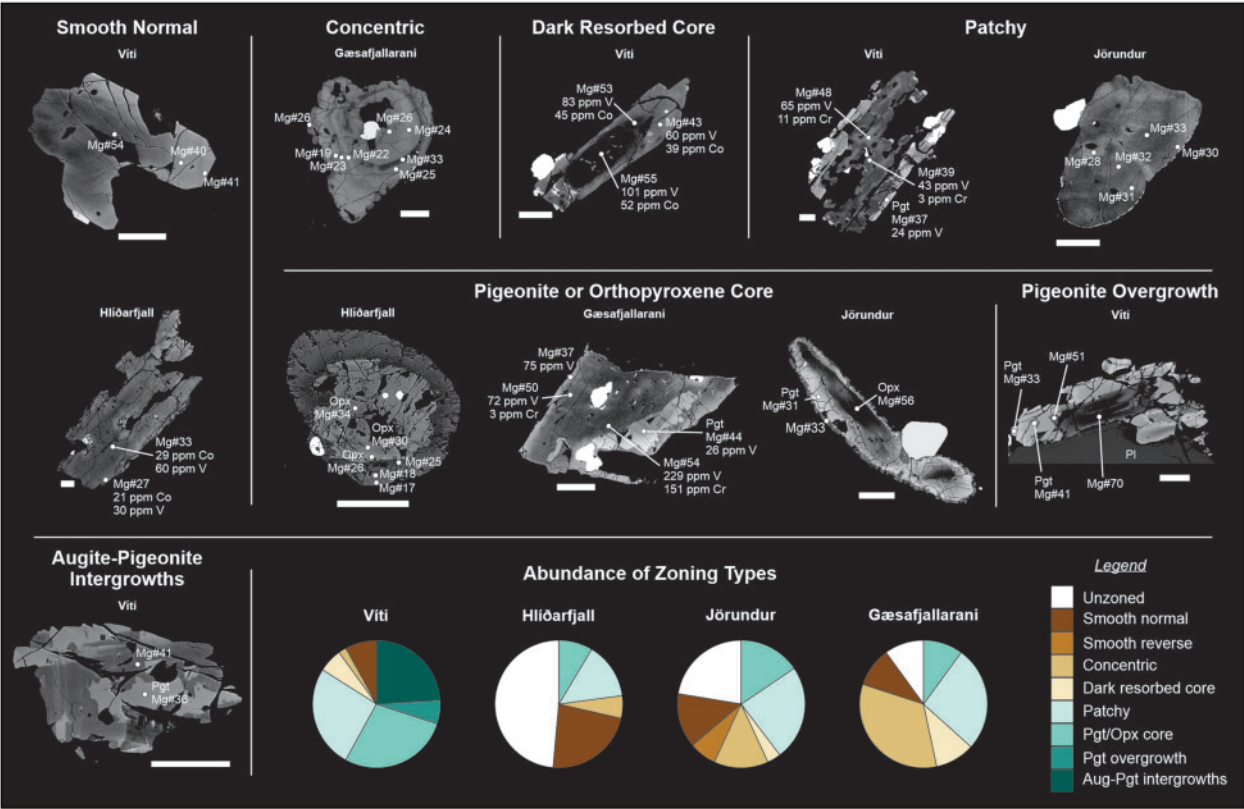
Fig. 7. Labelled BSE images of selected augite crystals (±pigeonite and/or orthopyroxene), highlighting different zoning types. Pie charts show the relative proportion of each zoning type within each unit. All analyses are augite unless specified: Pgt = pigeonite; Opx = orthopyroxene; Pl = plagioclase. Scale bars are 100 µm.

DISCUSSION

Our new dataset and microanalytical focus offer different perspectives with which previous models for the origin of Krafla rhyolites can be evaluated. Here, we first provide a brief overview of these previous models. We then consider the origin of the macrocrysts and their zoning patterns, before integrating our whole-rock and microanalytical datasets with insights from published
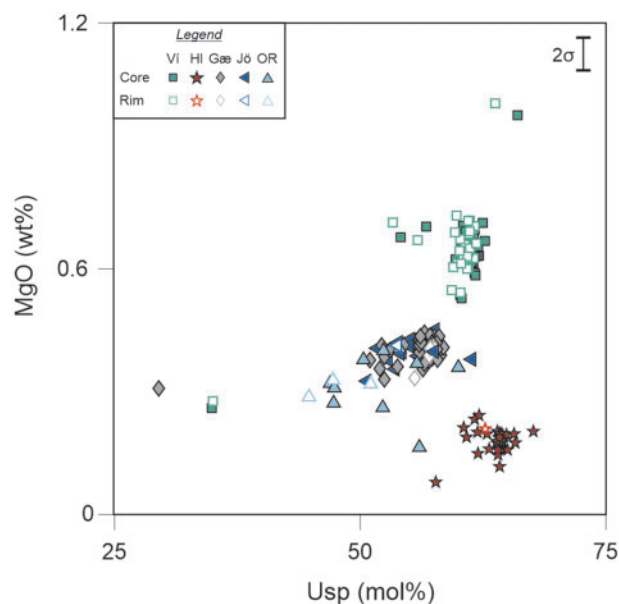
Fig. 8. MgO vs Usp for titanomagnetites. EPMA analyses recalculated after Carmichael (1967), mol% Usp calculated after Stormer (1983).

experimental work on partial melting of altered basalts and new major and trace element modelling. These constraints are linked into a conceptual model for the origin of Krafla rhyolites that is consistent with both the chemical and isotopic compositions of the rhyolites and the chemistries of their crystal cargoes.

Previous petrogenetic models
The origin of Krafla rhyolites has long been controversial. Whole-rock $\delta^{18}O$ and $(^{230}Th/^{232}Th)$ values are distinctly lower in the rhyolites than in the most primitive Krafla basalts, precluding their generation by simple closed-system fractional crystallization of the mantle-derived basalts that feed the system (Nicholson *et al.*, 1991; Sigmarsson *et al.*, 1991; Jónasson, 1994; Pope *et al.*, 2013; Hampton *et al.*, 2021). Instead, because the $\delta^{18}O$ of crustal rocks can be lowered by oxygen exchange between rocks and meteoric water in hydrothermal systems, petrogenetic models for the rhyolites have traditionally called on two endmember processes involving low-$\delta^{18}O$, hydrothermally altered crust: (1) a near-liquidus (crystallization-driven) process of assimilation-fractional-crystallization (AFC), whereby crystallizing basalts assimilate partial melts of altered basaltic crust as they crystallize (Nicholson *et al.*, 1991; Charreteur *et al.*, 2013), and (2) a near-solidus (melting-driven) process involving low-degree partial melting of hydrothermally altered basalts around the margins of basaltic magma chambers or intrusions, followed by extraction of these melts (Jónasson, 1994; Pope *et al.*, 2013; Zierenberg *et al.*, 2013).

More recently, Hampton *et al.* (2021) argued that the $\sim+2$ to $+3.5\%$ $\delta^{18}O$ values of Krafla rhyolite melts, although too low to reflect closed-system differentiation

of mantle-derived basalts ($\sim+5.5\%$), are too high to reflect pure partial melting of altered Krafla crust given the extremely low whole-rock values previously measured from altered borehole samples (-3.4 to -10.5%; Hattori & Muehlenbachs, 1982). Based on coupled thermal and thermodynamic modelling, and trace element fractional crystallization trends in zircons from the extra-caldera ridges, they instead proposed a two-step model for the generation of Krafla rhyolites. In this model, basaltic intrusions in high-temperature regions of the shallow crust assimilate altered material in an AFC process to produce low-$\delta^{18}O$ mafic to intermediate magmas. These magmas then segregate to shallower levels where they undergo further fractional crystallization with little to no further assimilation of low-$\delta^{18}O$ material.

Crystal perspectives on rhyolite petrogenesis
Origin of the crystal populations
The macrocryst populations of the rhyolites provide detailed records of processes occurring in their parental magmatic system, which can be used to evaluate previous models for rhyolite petrogenesis. A first step in decoding this crystal record is to test for equilibrium between the crystals and their carrier melt (for rims), or a hypothetical melt equivalent in composition to their host whole-rock (for earlier-formed cores).

Although commonly used as an equilibrium test for plagioclase, $K_D(An-Ab)^{plag-liq}$ values are highly sensitive to temperature and dissolved melt water content (Waters & Lange, 2015). We thus test for equilibrium by comparing observed compositions with plagioclase-liquid equilibrium pairs from experiments used to calibrate the Waters & Lange (2015) thermometer-hygrometer (Fig. 11a). Matrix glass compositions are not available for the oldest rhyolite or Gæsafjallarani due to pervasive devitrification; rims from the oldest rhyolite were therefore paired with the whole-rock composition, which closely approximates the carrier liquid due to the very low crystal content of this unit, whereas Gæsafjallarani rims, which are indistinguishable from Jörundur rims within analytical uncertainty, were paired with the average Jörundur glass composition. Most cores have compositions appropriate for equilibrium with a melt equivalent in composition to their respective whole-rock, although about 20% of cores from Víti and occasional cores from the other units are too calcic for equilibrium (Fig. 11a). All rim compositions are appropriate for equilibrium with their carrier melt, consistent with the euhedral forms of all grains and the relatively narrow, unimodal distributions of rim compositions for each unit, which both suggest an approach to equilibrium.

The K_D for Fe-Mg exchange between pyroxene and liquid is commonly used as an equilibrium test. Putirka (2008) proposes an equilibrium value of $K_D(Fe-Mg)^{cpx-liq} = 0.28 \pm 0.08$. However, the experimental data from which this value was derived are mainly from more mafic
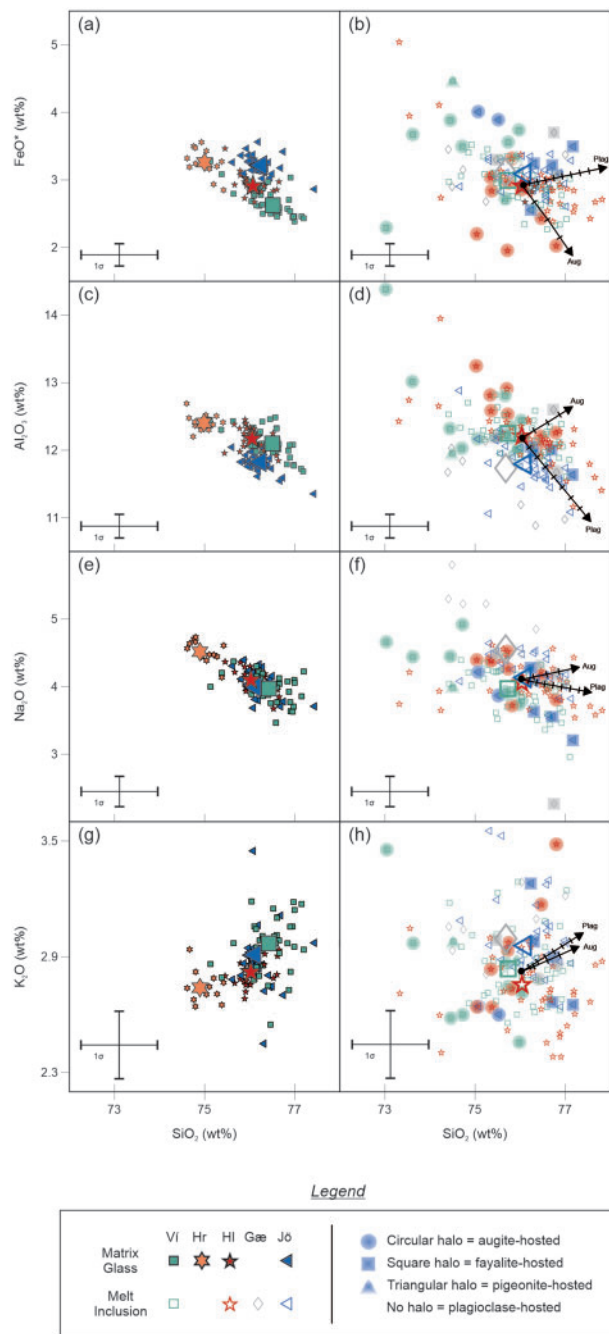
Fig. 9. Selected major element compositional plots for matrix glasses (left column) and melt inclusions (right column). All data are normalized anhydrous. Large symbols show the mean compositions for each unit; $2\sigma_M$ errors are smaller than the symbols. Black vectors show representative post-entrapment crystallization trends, assuming crystallization of augite (Mg#16; labelled Aug) or plagioclase (An$_{40}$; labelled Plag) from a representative melt inclusion (black circle); tick marks are 1% crystallization increments. Error bars show 1σ analytical error estimates based on replicate analyses of VG-568 rhyolite glass.

compositions, and K_D values are known to decrease with decreasing melt Mg# (e.g. Toplis & Carroll, 1995). To determine whether this value is applicable to low-Mg# rhyolitic melts, we calculated $K_D(Fe^{2+}\text{-}Mg)^{cpx\text{-}liq}$ values for augite-liquid pairs from phase equilibria experiments with

rhyolitic starting compositions and Mg#^{liq} <20 [where Mg#^{liq} = XMg/(XMg + XFe^{2+}), with XFe^{2+} calculated after Kress & Carmichael (1991); details of equilibrium K_D assessment are in Supplementary Data Spreadsheet S1]. The K_D values (n = 68, from seven experimental studies; Scaillet & Macdonald, 2003; Bolte et al., 2015; Almeev et al., 2012; Castro et al., 2013; Gardner et al., 2014; Brugman & Till, 2019; Huang et al., 2019) range from 0.03 to 0.41 with a strong mode around 0.14, a mean of 0.17, and standard deviation of 0.09. Hence, we test against the value of 0.17±0.09. Most augite cores are in or near equilibrium with melts equal in composition to their respective average whole-rock, and almost all rims are in equilibrium with the average groundmass glass (as before, pairing Gæsafjallarani rims with Jörundur glass) (Fig. 11b). For orthopyroxene, $K_D(Fe^{2+}\text{-}Mg)^{opx\text{-}liq}$ values from 19 experiments (Klimm et al., 2003, 2008; Castro et al., 2013; Huang et al., 2019) range from 0.07 to 0.37 with a prominent mode around 0.15, a mean of 0.21, and standard deviation of 0.09, hence we test for equilibrium against 0.21±0.09. The K_D formulation of Putrika (2008), which estimates the equilibrium K_D as a function of X$_{Si}$ of the melt, suggests values of 0.16±0.06 for melts equivalent to the average Krafla whole-rock composition for each unit, largely overlapping with our suggested equilibrium range. Almost all Víti orthopyroxene core and interior compositions are appropriate for equilibrium with a melt equivalent in composition to the average Víti whole-rock (Fig. 11c). Compositions from Jörundur and Hlíðarfjall fall outside of the equilibrium range, but many are close and have compositions appropriate for equilibrium with silicic melts similar to the Víti rhyolite (i.e. Mg# <15).

These equilibrium tests indicate that most macrocrysts derive from evolved melts similar to, or only slightly more primitive than, their carrier liquid. The scarce augite and orthopyroxene cores and interiors from Jörundur and Víti with Mg# >60 probably derive from mafic or intermediate melts; elevated concentrations of highly compatible trace elements in some of the most primitive augites and orthopyroxenes (e.g. 134 and 151 ppm Cr in two augite analyses from Gæsafjallarani with Mg# 58 and 54; 453 ppm Cr in one augite from Víti with Mg# 63), indicate growth from mafic (probably basaltic) melts not yet depleted in strongly compatible elements.

Apparent equilibrium between most crystal cores and liquids equivalent to their host whole-rock could suggest that most grains are true phenocrysts native to their carrier magma. However, several features point to a more complex scenario:

1. Trace element variability within crystal populations of individual units far outweigh the variability within individual grains and commonly show only modest correlation with major element compositions (e.g. Sr in plagioclase; Fig. 5), suggesting mixing of crystals from multiple sources or sub-regions of a poorly mixed reservoir.
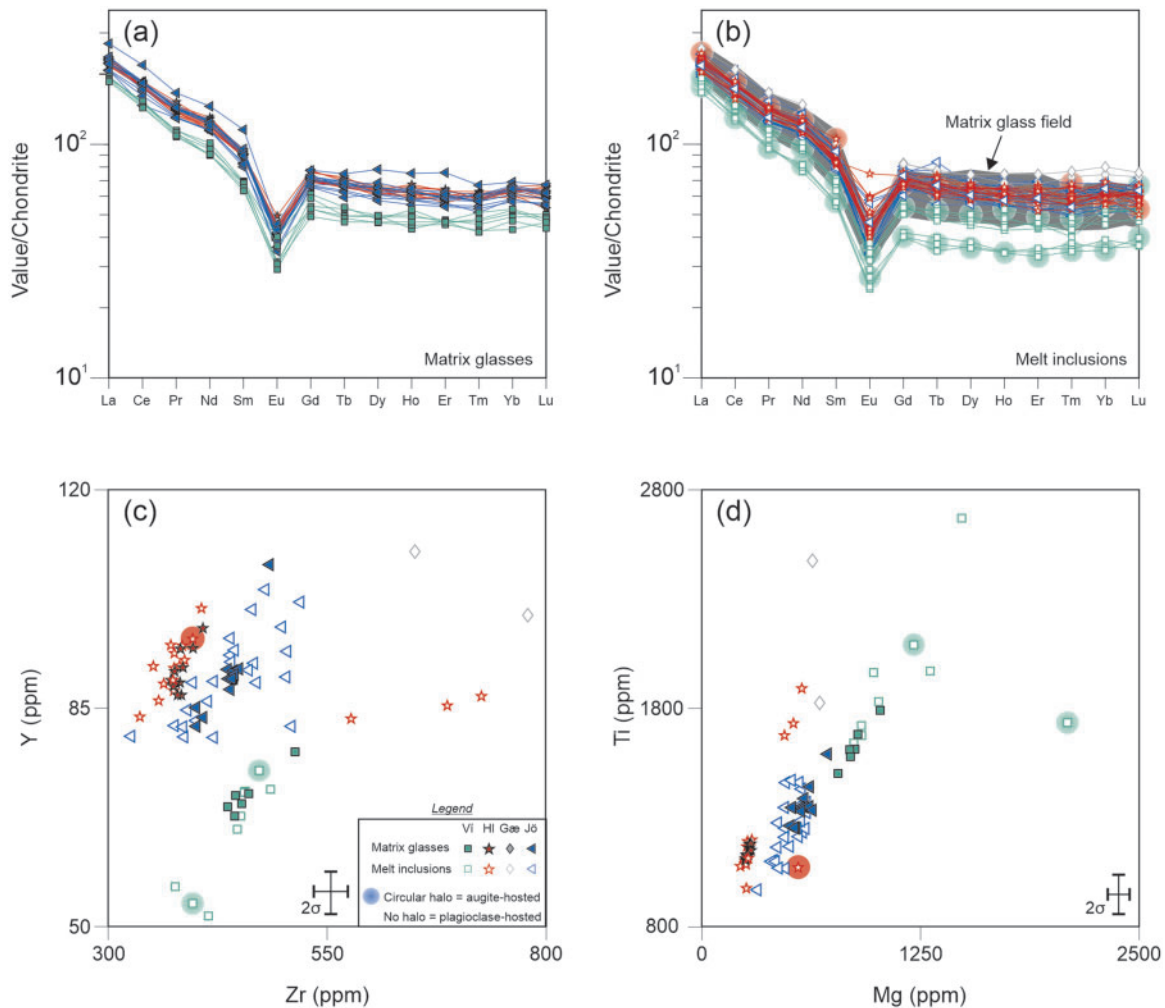
Fig. 10. Selected trace element compositional plots (determined by LA–ICP–MS) for matrix glasses and melt inclusions. Data in (a) and (b) are normalized to the chondrite value of McDonough & Sun (1995). Analytical uncertainties (2σ) were estimated based on relative errors for replicate analyses of BCR-2G.

2. The crystal populations of each unit show complex and diverse growth histories. Crystals with both normal and reverse net core-rim zoning are juxtaposed, and many host interior resorption surfaces. High- and low-Ca pyroxenes commonly have inherited cores of the alternate phase (Figs 5 and 7).
3. Melt inclusion populations from each unit show greater scatter than matrix glasses (Fig. 9) and include values that fall off the main trends for trace elements (Fig. 10c and d), suggesting entrapment of compositionally diverse evolved melts. Although most major element analyses are within 2σ analytical uncertainty of the corresponding matrix glass field, the tighter clustering of matrix glasses analysed in the same sessions suggests that the apparent compositional diversity of the melt inclusions is at least partly a real feature. Occasional melt inclusions are more primitive than matrix glasses and enriched in elements compatible in the observed mineral assemblages (e.g. Sc, Zr, Hf, Ti, Mg, and Eu; Fig. 10), indicating entrapment of less-evolved rhyolitic melts during an earlier stage of magmatic

differentiation. In contrast, some inclusions are more evolved than matrix glasses and largely cluster off the expected trends for post-entrapment crystallization (Fig. 9), suggesting that some crystals entrapped liquids more evolved than their current carrier melt.

From these lines of evidence, we infer that while some macrocrysts in the Krafla rhyolites may represent true phenocrysts that nucleated and grew entirely in their current host melt, most grains have experienced more complex and diverse histories. We thus interpret the cores ± interiors of many grains as antecrystic material derived from diverse silicic (broadly dacitic to rhyolitic) sources and mixed or assimilated into a final common melt in which they experienced further rim growth before eruption. This mixing of macrocrysts with diverse histories is consistent with variable and non-correlated $\delta^{18}O$ and trace element contents in zircons from the extra-caldera ridge rhyolites, interpreted by Hampton *et al.* (2021) to reflect mixing of zircons from multiple poorly connected regions of an
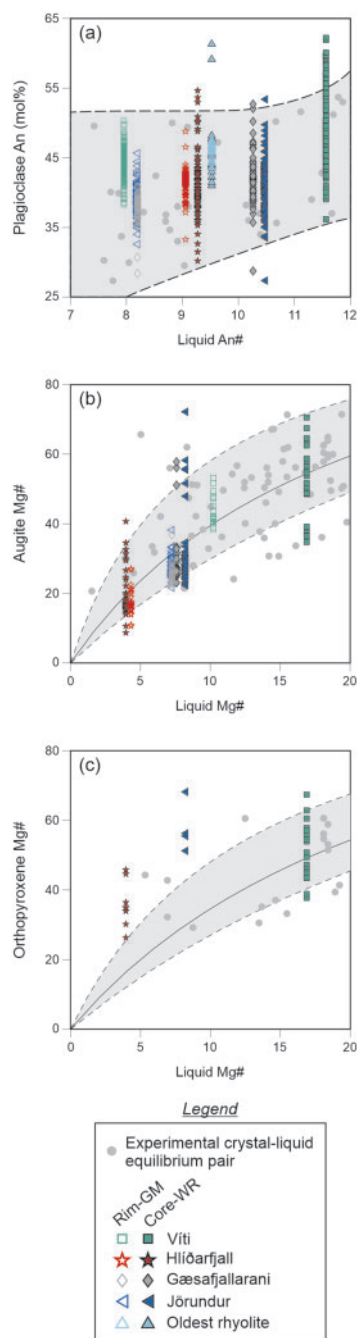
Fig. 11. Equilibrium tests for macrocrysts in Krafla rhyolites. Cores (plus interiors for orthopyroxene) were paired with the average whole-rock (WR) composition and rims paired with the average matrix glass (GM) composition for their respective unit (rims paired with whole-rock composition for the fully devitrified oldest rhyolite). Equilibrium crystal-liquid pairs from phase equilibria experiments on rhyolitic compositions are shown as grey dots. (a) Tests for plagioclase. Liquid An# is calculated after Waters & Lange (2015). The grey shaded field encloses all experimental plagioclase-liquid equilibrium pairs (grey dots) used to calibrate the Waters & Lange (2015) plagioclase-melt thermometer-hygrometer across the range of liquid An# shown. (b) Rhodes diagram for augite. Grey shaded envelope shows equilibrium pyroxene compositions for a given melt Mg# assuming $K_D(Fe^{2+}\text{-}Mg)^{cpx\text{-}liq} = 0.17 \pm 0.09$ and melt $Fe^{3+}/\Sigma Fe = 0.2$ (see text). (c) Rhodes diagram for orthopyroxene. Grey shaded envelope shows equilibrium pyroxene compositions, assuming $K_D(Fe^{2+}\text{-}Mg)^{opx\text{-}liq} = 0.21 \pm 0.09$ and melt $Fe^{3+}/\Sigma Fe = 0.2$ (see text).

isotopically heterogeneous silicic reservoir. Hence, both the macrocryst and zircon populations of the Krafla rhyolites appear to support mixing of chemically (and isotopically) diverse silicic components. Similar or even more pronounced diversities in trace element and isotopic compositions are common in zircon populations of other Icelandic rhyolites (Carley *et al.*, 2011; Bindeman *et al.*, 2012; Banik *et al.*, 2018), suggesting that the mixing and/or recycling of silicic components captured by crystal populations in the Krafla rhyolites may be typical of many Icelandic rhyolites.

### Crystal zoning as a record of late-stage magma assembly and evolution

The compositions of growing magmatic crystals are sensitive to both intensive variables (e.g. pressure, temperature) and melt compositions. Hence, crystal zoning patterns can provide a detailed record of pre-eruptive processes and changing magmatic environments during magma storage, assembly and differentiation. Here we further probe this record to shed light on the origin of the Krafla rhyolites and their diverse crystal populations.

The dominance of normal core-rim zoning among plagioclase and augite populations (Figs 4 and 6) and rim-ward decreases in compatible element concentrations (e.g. Co and V in pyroxenes; Fig. 7) are consistent with a general trend of crystal growth from progressively evolving melts. The minority of grains that are reverse-zoned overall host internal resorption surfaces, with outer mantles that are normally zoned out to the rim (e.g. many dark resorbed core types; Fig. 5). Together with the occasional presence of melt inclusions that are more primitive than matrix glasses, we interpret these first-order observations as evidence for crystallization-driven differentiation (i.e. fractional crystallization) of the silicic melts from which the rhyolites were ultimately assembled.

Despite the general trend towards normal zoning, especially in the outer regions of crystals approaching their rims, the internal zoning patterns in many plagioclase and pyroxene crystals reflect variable and complex magmatic histories involving changing physical and/or chemical conditions and periods of disequilibrium between crystals and melt. For plagioclase, the fine-scale oscillatory zoning with small chemical oscillations (<2–3 mol%) shown by the 'subtle oscillatory' type (Table 4) can be attributed to kinetic effects in a local boundary layer between the growing crystal and melt, but larger abrupt compositional shifts and internal resorption surfaces require a different process or processes (e.g. Ginibre *et al.*, 2002*a*).

For melt of a given composition, the An content of crystallizing plagioclase is positively correlated with both temperature and P_{H2O} (e.g. Waters & Lange, 2015). Hence, in a magma body closed to recharge, fluctuations in plagioclase An content can relate to (1) temperature variations related to thermal convection (Couch *et al.*, 2001), or (2) multiple stages of ascent and
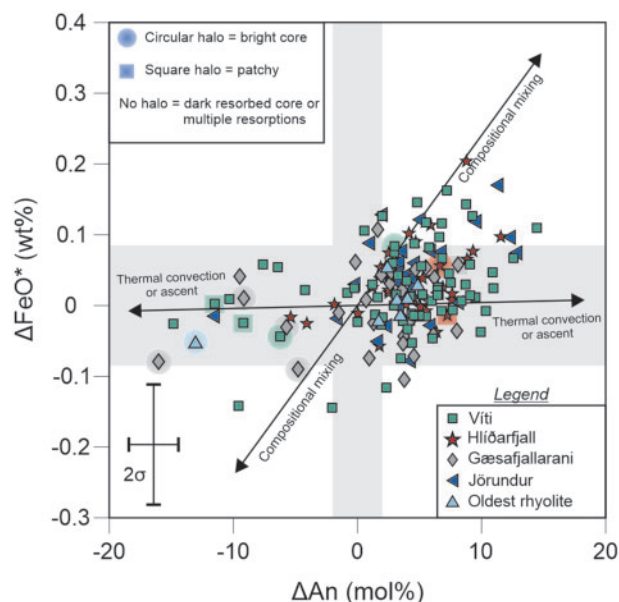
Fig. 12. Compositional changes across plagioclase internal resorption surfaces. ΔAn = change in plagioclase An (mol%; outer zone—inner zone). ΔFeO^* = change in total Fe expressed as FeO (wt; outer zone—inner zone). Compositional mixing and thermal convection or ascent vectors after Ruprecht & Wörner (2007). Compositional changes plotting within the grey fields are less than the 2σ analytical uncertainty.

decompression, possibly with resultant degassing of H_2O (e.g. Humphreys *et al.*, 2006). Alternatively, open system processes involving magma mixing and/or thermal rejuvenation of near- or sub-solidus intrusions by hot recharge magma can cause abrupt changes in An content, possibly accompanied by crystal resorption. In the typical case where recharge magmas are compositionally distinct (usually more mafic than the resident magma), Fe concentrations provide a useful means to identify open system processes because Fe incorporation into plagioclase primarily depends on melt composition (e.g. Ginibre *et al.*, 2002*b*; Lundgaard & Tegner, 2004). Small differences in Fe partitioning can result from slight changes in fO_2 during closed-system differentiation and degassing, but large and correlated Fe-An shifts imply mixing between compositionally distinct magmas (e.g. Ruprecht & Wörner, 2007).

Compositional contrasts in An content and FeO* across major plagioclase resorption surfaces are plotted in Fig. 12. Most resorption events, corresponding mainly with 'dark resorbed core' or 'multiple resorption' type zoning patterns (Table 4), show An increases of <10 mol% and no resolvable change in Fe within 2σ uncertainty. Only 12% of resorption surfaces show a coupled increase in Fe and An (>2σ analytical uncertainty) consistent with incorporation into a more mafic melt. Augite macrocrysts similarly lack resorption surfaces or sharp compositional boundaries corresponding with large and coupled increases in Mg# (>10) and compatible element concentrations (e.g. Sc, V, Cr, Co), indicative of mixing with mafic recharge magma (e.g.

Astbury *et al.*, 2018; Ubide & Kamber, 2018). Those crystals that do show textural evidence for large and abrupt compositional shifts (Mg# >10) or major resorption events ('dark resorbed core', 'patchy', and some 'concentric' types) are normally zoned across these boundaries. We thus infer that the late-stage evolution of the Krafla rhyolites occurred largely in isolation from the underlying mafic system, and most crystals did not experience compositional mixing with mafic recharge magmas. The small number of resorbed pyroxene cores with Mg# >60 and high Cr contents could conceivably derive from intruding basaltic magmas, but the lack of evidence for such recharge events in the other crystals indicates that they more probably reflect minor assimilation of basaltic restite or wallrock. A small number of plagioclase crystals (9%), including 'patchy', 'bright core', and 'multiple resorption' types, show decreases in An content, which are usually decoupled from any detectable change in Fe. These events may reflect plagioclase resorption during ascent of a water-undersaturated melt (e.g. Holtz *et al.*, 2001), followed by water exsolution and overgrowth of more sodic compositions once saturation is achieved at shallower depths (Humphreys *et al.*, 2006).

As an alternative to closed-system processes, some plagioclase resorption events may reflect assimilation and partial resorption of antecrysts derived from silicic mush or intrusives; Fe contents in plagioclase are insensitive to such changes because of the similar Fe contents of the assimilant and melt. Direct evidence for partial remelting and assimilation of hypabyssal silicic intrusive rocks (termed 'felsite' in recent publications) near the roof of the IDDP-1 rhyolite body at Krafla has been documented in materials sampled during drilling (Zierenberg *et al.*, 2013; Masotta *et al.*, 2018; Saubin *et al.*, 2021). We infer that much of the diversity in compositions and zoning patterns of the erupted Krafla rhyolites reflects a similar reprocessing of silicic intrusives or mush in the shallow crust.

Experimental and modelling perspectives on rhyolite petrogenesis

The recycling of near- or sub-solidus silicic intrusions and/or mixing of discrete silicic magma batches appear to play important roles in assembly of the final erupted magmas, but must be secondary processes in the generation of Krafla rhyolites because they involve existing differentiated components. Ultimately, the central differentiation processes that drive the production of these silicic components at Krafla must be dominated either by crystallization (i.e. AFC, *sensu* Nicholson *et al.*, 1991; Hampton *et al.*, 2021) or melting (*sensu* Jónasson, 1994; Pope *et al.*, 2013). The recent isotopic arguments of Hampton *et al.* (2021) appear to render the latter unlikely; because oxygen isotope fractionation is very limited during crustal melting, producing the Krafla rhyolites by partial melting requires a source with a similar $\delta^{18}O$ to the rhyolites themselves (~+2 to +3.5‰) and much
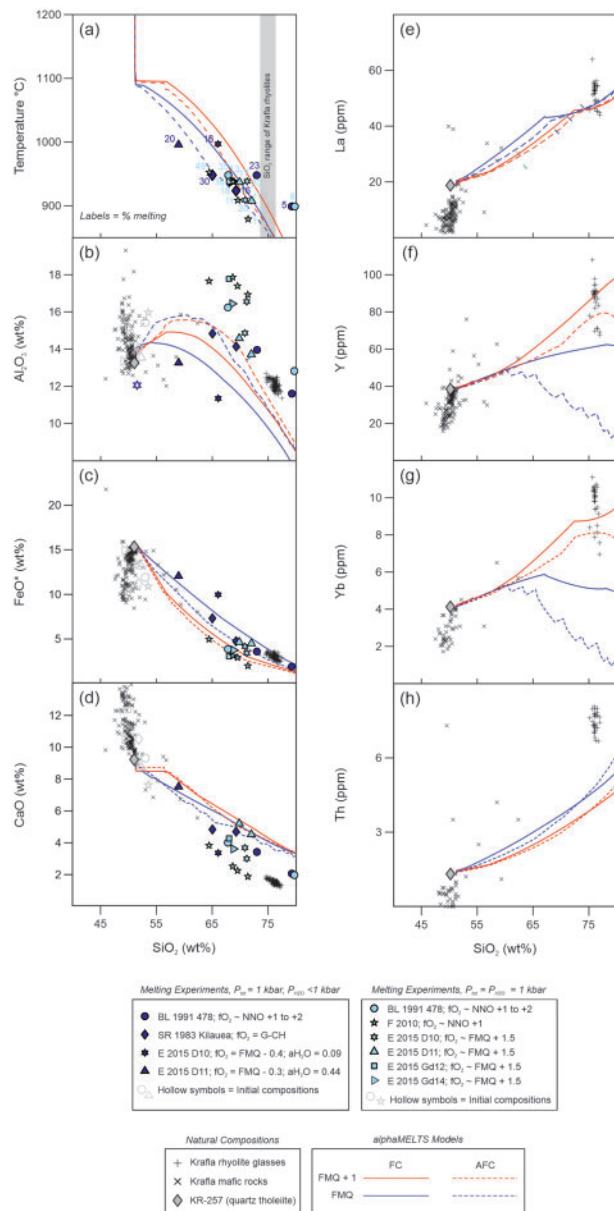
Fig. 13. Selected MELTS major and trace element models for rhyolite petrogenesis by pure FC or AFC from initial composition of KR-257 (evolved quartz tholeiite basalt from the Halarauður eruption; Rooyakkers, 2020), assuming an initial H_2O content of 1 wt%. All models are run from above liquidus at 1 kbar total pressure. AFC models are isenthalpic, with hydrated KR-257 (3 wt% H_2O) as the assimilant. Major element compositions of experimental partial melts produced from hydrated or altered basalts and metabasalts are shown for water-undersaturated (dark blue) and water-saturated (light blue) conditions and 1 kbar total pressure. Data for Krafla mafic rocks are from Grönvold & Mäkipää (1978), Nicholson (1990), Hemond et al. (1993), Jónasson (1994) and Cooper et al. (2016). SR 1983 = Spulber & Rutherford (1983); BL 1991 = Beard & Lofgren (1991); F 2010 = France et al. (2010); E 2015 = Erdmann et al. (2015).

higher than published values for altered Krafla basalts. Instead, Hampton *et al.* (2021) successfully produced isotopic compositions similar to the Krafla rhyolites in energy-constrained AFC models involving assimilation

of partial melts from altered low-$\delta^{18}O$ basaltic wallrocks, although further additional fractional crystallization in the absence of assimilation was required to produce evolved rhyolitic melts. Trace elements were not considered in these models.

The isotopic arguments and modelling of Hampton *et al.* (2021) are underpinned by the assumption that the extremely low $\delta^{18}O$ values reported from altered Krafla borehole samples (−3.4 to −10.5‰; Hattori & Muehlenbachs, 1982) are representative of the average altered Krafla crust at the depths of silicic magma generation. This appears to be a reasonable assumption, but is difficult to prove with available data. Here we consider two alternative perspectives to shed further light on the viability of crystallization-driven versus melting-driven processes for generating Krafla rhyolites: (1) published experimental work on partial melting of altered basalts and metabasalts, and (2) trace element models for crystallization-driven processes (FC and AFC).

Experimental melting of altered basalts

Central to partial melting models for the origin of Krafla rhyolites are their Fe-rich and Al- and Ca-poor compositions, which resemble low-degree partial melts of hydrated basalts or metabasalts produced experimentally at $P_{H2O} < 1$ kbar and $P_{total} = 1$–3 kbar (Spulber & Rutherford, 1983; Thy *et al.*, 1990; Beard & Lofgren, 1989, 1991). Jónasson (1994) also argued for melting at fO_2 values below the fayalite-magnetite-quartz (FMQ) buffer, but we note that only the Spulber & Rutherford (1983) experiments were run at these reducing conditions. More recent low-pressure melting experiments on altered basaltic or gabbroic rocks have produced melts similar to Icelandic rhyolites at relatively oxidizing conditions more appropriate for hydrothermally altered materials [fO_2 on or above the nickel–nickel oxide (NNO) buffer; Koepke *et al.*, 2004; France *et al.*, 2010; Erdmann *et al.*, 2015], and we suggest that the fO_2 constraint can be relaxed. Nonetheless, because of its strong effect on plagioclase stability, low P_{H2O} is especially important in the partial melting model. Because of the greater stability of plagioclase relative to mafic phases in the source, melting at low P_{H2O} forms silicic melts that are rich in Fe and poor in Al and Ca, similar to Icelandic rhyolites (Spulber & Rutherford, 1983; Beard & Lofgren, 1989, 1991; Thy *et al.*, 1990).

Despite the compositional similarities between the Krafla rhyolites and some experimental melts, certain features of the experimental results hint at difficulties in producing the observed rhyolite compositions and volumes purely by melting. First, because of the breakdown of hydrous alteration minerals and the relatively low solubility of H_2O in silicic melts at low pressure, experimental melts of hydrothermally altered basaltic rocks at low pressure (1–2 kbar) may in some cases reach water saturation regardless of whether excess water is added to the experimental charge or not (e.g. France *et al.*, 2010). Thus, at low pressure, even

Table 6: Summary of MELTS fractional crystallization and AFC models

| Model	Starting composition	fO_2 Buffer	Assimilant	R (mass of cumulates/ mass assmilated) at 75 wt% SiO_2	f (mass fraction of remaining melt) at 75 wt% SiO_2	Temperature (°C) at 75 wt% SiO_2	Crystallizing assemblage at 75 wt% SiO_2
FC	KR-257, 1wt% H_2O	FMQ+1	–	–	0.33	894	70.3% plag, 9.1% aug, 7.6% opx, 5.9% rhm-ox, 3.7% sp, 3.4% ap
FC	KR-257, 1wt% H_2O	FMQ	–	–	0.28	867	68.1% plag, 9.5% aug, 8.6% pgt, 11.2% sp, 2.6% ap
AFC	KR-257, 1wt% H_2O	FMQ+1	KR-257, 3 wt% H_2O, 500°C	1.37	0.33	865	64.4% plag, 12.5% aug, 10% opx, 9.9% sp, 1.3% rhm-ox, 1.3% ap
AFC	KR-257, 1wt% H_2O	FMQ	KR-257, 3 wt% H_2O, 500°C	1.27	0.32	857	25.1% aug, 60.1% plag, 14.1% sp, 0.7% ap

plag = plagioclase, aug = augite, pgt = pigeonite, opx = orthopyroxene, rhm-ox = rhombohedral oxide, sp = spinel, ap = apatite.

pure dehydration melting of altered basaltic rocks, where only structural water in hydrous minerals is available for melting reactions, can destabilize plagioclase and produce melts in equilibrium with a water-rich fluid (i.e. $P_{H2O} \sim P_{total}$, aH_2O close to 1), which have higher Al contents than Icelandic rhyolites. Second, the experimental results reveal difficulties in producing significant volumes of evolved rhyolitic compositions with >75 wt% SiO_2; the required melt fractions are low (generally <10%) and restricted to a narrow temperature window (<~50°C) near the solidus, and some experiments failed to produce such evolved compositions at all (Fig. 13). Hence, even though the bulk melt composition produced by low-degree partial melting of altered basalts is undoubtedly silicic, we infer that significant volumes of evolved rhyolite with ~75 wt% SiO_2 are unlikely to be generated by this melting process alone. Explaining the origin of the largest rhyolitic magma batches produced at Krafla, such as the >0.5 km³ (possibly >5 km³) involved in the Halarauður eruption, by such a process is particularly difficult, requiring low degrees of melting within this optimal temperature window across an approximately tenfold greater volume of crust.

Most melts produced in these experiments are dacites to low-silica rhyolites, which form across a window of approximately 10–40% melting (Fig. 13). This raises the possibility that rhyolites at Krafla derive from less-evolved silicic partial melts, which subsequently differentiate to more evolved compositions by fractional crystallization ± assimilation (see Sigmarsson *et al.*, 1991, 1992; Martin & Sigmarsson, 2010). Such a model would be consistent with the dominance of crystals entirely derived from evolved (broadly silicic) magmas and the general trends of progressive differentiation shown by crystal zoning patterns in the rhyolites, but suffers from the same isotopic limitations as the pure partial melting model unless the $\delta^{18}O$ of the altered crust is similar to the final magma (see Hampton *et al.*, 2021).

Modelling of rhyolite petrogenesis

To explore the viability of protracted AFC from a basaltic parent in generating the Krafla rhyolites, we use alphaMELTS v.1.9 (Smith & Asimow, 2005), implementing the MELTS algorithm of Ghiorso and Sack (1995), to calculate a liquid line of descent. All alphaMELTS input and output files are included in the Supplementary Data Material. Our ability to forward model a partial melting scenario is limited by a lack of quantitative petrologic data from altered Krafla (or similar Icelandic) basalts (e.g. bulk trace element compositions, compositions and modal proportions of igneous and alteration minerals), and the inability of MELTS to model hydrous hydrothermal or metamorphic phases and kinetic effects (see Troch *et al.*, 2018, for a broader discussion). Given these caveats, we do not attempt to model partial melting with alphaMELTS, but stress the need for new
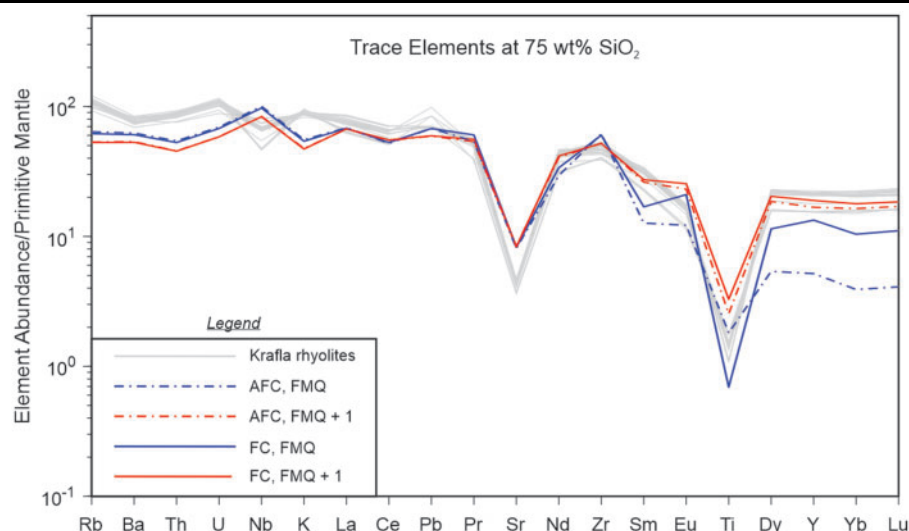
Fig. 14. Trace element spider diagram for MELTS FC and AFC models at 75 wt% SiO_2, compared to Krafla rhyolite matrix glass compositions. All data are normalized to primitive mantle values of Sun & McDonough (1989).

experimental work to shed light on the melting behaviour of altered Icelandic basalts.

Isenthalpic AFC models are generated using a whole-rock analysis of sample KR-257, an evolved quartz tholeiite basalt from the Halarauður eruption, as the starting composition. This composition approximates a magmatic liquid due to the sample's low crystal content (<2 modal%), and is representative of the evolved, crystal-poor quartz tholeiites with ~5–6 wt% MgO typical of the central volcano (Nicholson, 1990), including those erupted in the historic Mývatn and Krafla Fires episodes (Grönvold, 1984; Cooper et al., 2016). We assume 1 wt% H_2O, a typical value for the most evolved Icelandic basalts (Nichols et al., 2002; Guilbaud et al., 2007). Hydrated KR-257 with 3 wt% H_2O is used as the assimilant, with an assumed initial temperature of 500°C. Magnetite-ilmenite oxygen barometry by Nicholson (1990) yielded fO_2 estimates for Krafla basalts close to the FMQ buffer, but recent studies have proposed more oxidizing conditions for Icelandic basalts, reaching up to FMQ + 0.6 for basaltic glasses from the Reykjanes Ridge (Shorttle et al., 2015), and FMQ + 0.7±0.1 for evolved basalts from Laki and Holuhraun (Hartley et al., 2017; Halldórsson et al., 2018). We thus buffered fO_2 at either FMQ or FMQ + 1. All models use composition- and temperature-dependent partition coefficients for plagioclase and clinopyroxene calculated after Blundy & Wood (1994) and Wood & Blundy (1997), respectively. Partition coefficients for REE in apatite are from Fujimaki (1986). For comparison with AFC, pure FC models (i.e. without assimilation) are also run with the same starting conditions.

Our alphaMELTS FC and AFC forward models match the compositions and phase assemblages of the natural rhyolites reasonably well (Figs 13–15; Table 6). All models over-predict melt CaO contents for the rhyolitic compositions (probably due to under-stabilization of clinopyroxene, a known limitation of MELTS; Fowler &

Spera, 2010; Gleeson et al., 2017), and under-predict K_2O contents by up to ~1 wt%. Despite these shortcomings, we consider the overall fit to be good for the major elements, particularly for the AFC models. Reasonably good fits to the observed trace element compositions are also produced by the three FC models and the most oxidizing AFC model, which predict large negative Sr and Ti anomalies and REE + Y concentrations similar to the natural samples (Fig. 14). Predicted mineral assemblages at 75 wt% SiO_2 for the FC models are in reasonable agreement with observed assemblages (Table 6, Fig. 15; cf. Table 2). None of the models predict quartz or alkali feldspar until near the solidus, consistent with their absence in the Krafla rhyolites.

A new petrogenetic model for rhyolites and origin of the Daly gap at Krafla

In detail, the process that ultimately produces Krafla rhyolites is undoubtedly more complex than the end-member processes that we have modelled; our micro-analytical data indicate additional complexities involving mixing of distinct silicic magma batches and/ or remobilization of felsic intrusions. For these reasons, as well as the inherent limitations and assumptions involved in geochemical modelling, it is unsurprising that none of our models capture all compositional features of the Krafla rhyolites. Nonetheless, many such features are reproduced well, and provide important insights on the likely processes that drive rhyolite production at Krafla.

The good fit for most of our MELTS models to the observed major and trace element compositions points towards a dominant role for crystal fractionation in the generation of Krafla rhyolites. The assumption of isenthalpic (heat-balanced) conditions results in a relatively large assimilated component in the final magmas; predicted R values (mass of magma crystallized/mass of
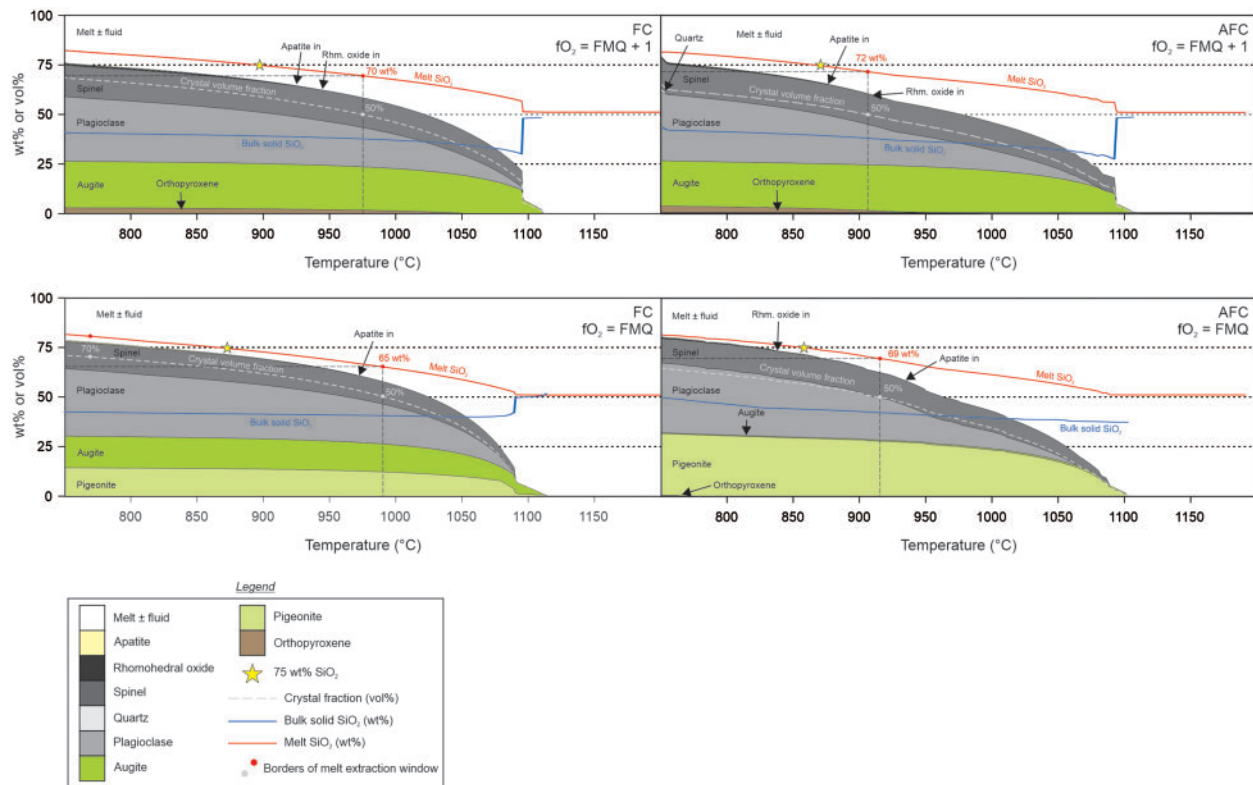
Fig. 15. Plots showing mass proportions of cumulus phases and residual melt (±exsolved fluid) predicted by MELTS as a function of temperature in FC and AFC models. The arrivals of minor phases (e.g. apatite) are marked with arrows for clarity. The total fraction of crystals (in vol%) is shown with grey dashed curves, and SiO_2 contents of melts and bulk solids (in wt%) are shown as red and blue solid curves, respectively. Melt SiO_2 contents of 75 wt%, similar to Krafla rhyolites, are marked with a yellow star. Hexagons on the melt SiO_2 and crystal volume fraction curves mark the boundaries of the 50–70% crystallinity range, identified by Dufek & Bachmann (2010) as the optimal window for melt extraction from crystal mushes.

assimilated crust) once the melt reaches 75 wt% SiO_2 are ∼1.27–1.37 (Table 6). This assumption, however, is likely to be a poor approximation for conditions in the shallow crust at Krafla, where a large fraction of magmatic heat is transferred to its vigorous hydrothermal system (Eichelberger, 2020). Interestingly, however, the pure FC models provide equally good or better fits to the observed trace element contents that the AFC models, implying that relatively modest assimilation of altered mafic crust is also consistent with the observed trace element compositions. The change in melt $\delta^{18}O$ during AFC can be modelled by:

$$\delta^{18}O_m = \delta^{18}O_0 + [(\delta^{18}O_a - \delta^{18}O_0) - \Delta^{18}O_{crystals-melt} * R] * [1 - f^{\wedge}1/(R - 1)]$$

where $\delta^{18}O_m$, $\delta^{18}O_0$, and $\delta^{18}O_a$ are the $\delta^{18}O$ values of the final magma, parent magma, and assimilant, respectively, $\Delta^{18}O_{crystals-melt} = \delta^{18}O_{crystals} - \delta^{18}O_{melt}$, and f is the mass fraction of remaining liquid (White, 2013). Our MELTS models predict f values between 0.28 and 0.33. Taking f = 0.3 and assuming $\delta^{18}O_0 = +5‰$ (Hampton *et al.*, 2021), $\delta^{18}O_a = -5‰$ (Hattori & Muehlenbachs, 1982), and $\Delta^{18}O_{crystals-melt} = -0.5‰$, a final melt $\delta^{18}O$ of $+2‰$ requires an *R* value of ∼3.7. For $\delta^{18}O_a = 0‰$ this reduces to ∼1.9. Hence, we suggest that

major, trace element, and isotopic compositions of Krafla rhyolites are all consistent with generation from evolved quartz tholeiite melts by a fractional-crystallization-dominated process involving either modest assimilation of highly altered crust ($\delta^{18}O_a \sim -5‰$) or high-degree assimilation of moderately altered crust ($\delta^{18}O_a \sim -0‰$).

It is now broadly accepted that the generation of crystal-poor rhyolites by crystal fractionation involves extraction of interstitial melt from crystal mushes (Bachmann & Bergantz, 2004; Hildreth, 2004). This occurs after the mush reaches rheological lockup at ∼40–50% crystallinity (Bachmann & Bergantz, 2004), and is most efficient once crystallinities of ∼50–70% are reached (Dufek & Bachmann, 2010). For most elements, the process of mush formation and melt extraction can be modelled as fractional crystallization because diffusion in crystalline phases is too slow to maintain equilibrium even in slowly crystallizing mushes (see Gelman *et al.*, 2014, for discussion). At temperatures appropriate for silicic magmas, diffusion coefficients in crystalline phases are commonly $<10^{-20}\, m^2\, s^{-1}$ (Gelman *et al.*, 2014, and references therein), such that characteristic diffusion times for 1 mm-diameter crystals are of the order of 10^6 years or more, much longer than the lifespan of the Krafla system. Assuming
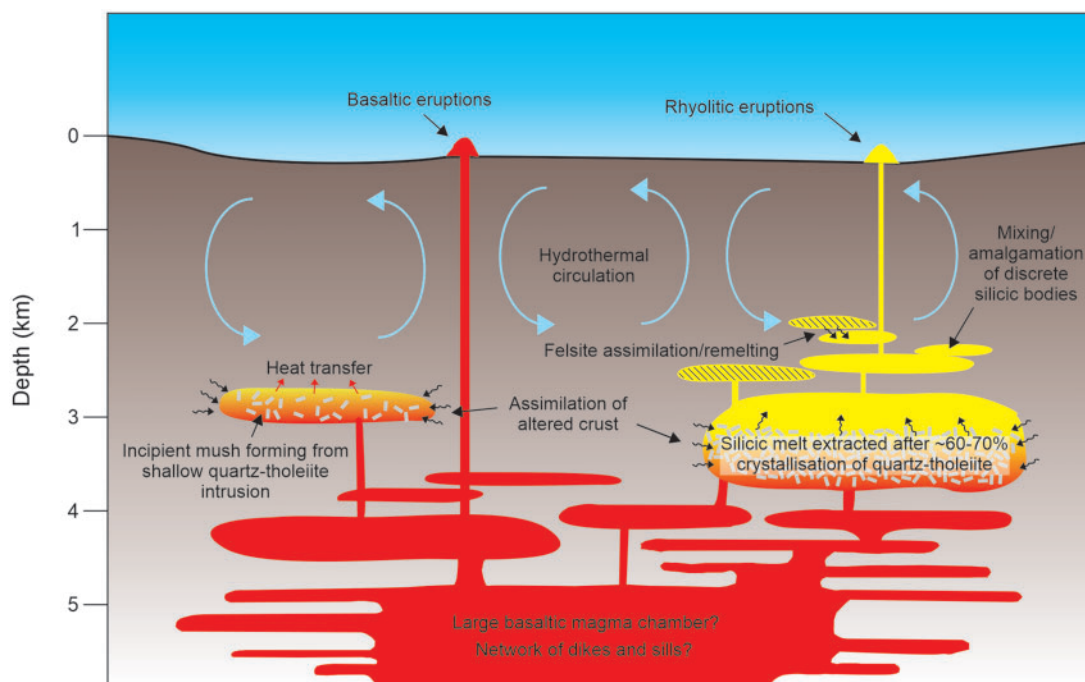
Fig. 16. Conceptual model for rhyolite petrogenesis at Krafla. Evolved, crystal-poor quartz tholeiite bodies stall and crystallize in the shallow crust (∼3–4 km deep), assimilating low-δ^{18}O crust in an AFC process. Crystal mushes formed by this process host evolved interstitial melt with compositions similar to the Krafla rhyolites after ∼55–65% crystallization by volume. These evolved melts are extracted from their source mush bodies, leaving mafic cumulates at depth. The extracted melts ascend to ∼2–3 km deep where they may mix with other extracted silicic magma batches and/or remobilize and assimilate compositionally similar silicic mush or intrusives. The diverse macrocryst populations of the rhyolites reflect this mixing and reprocessing of compositionally similar silicic material. The resulting crystal-poor rhyolite magmas either erupt, or stall and solidify at depth to form silicic intrusions that may later be remelted and recycled in similar fashion.

complete and instantaneous removal of crystals from melt as we have done here is akin to assuming instantaneous extraction and separation of the interstitial melt after an extended period of closed-system fractional crystallization, during which the crystal interiors are removed from contact with the melt by continual rim growth and do not re-equilibrate with the melt due to sluggish intracrystalline diffusion.

For all MELTS models, silicic melts reaching at least ∼75 wt% SiO_2, similar to the natural compositions, occur after ∼55–65 vol% crystallization, overlapping with the ∼50–70% crystallinity window in which melt extraction from crystal mushes is most efficient (Dufek & Bachmann, 2010) (Fig. 15). We thus propose that rhyolitic melts at Krafla form when evolved, crystal-poor quartz tholeiites typical of the central caldera region are emplaced and undergo extensive crystallization at shallow levels (∼1 kbar), eventually forming mush bodies with interstitial silicic melt (Fig. 16). Assimilation of variably altered, low-δ^{18}O basaltic crust occurs around the margins of the developing mushes, lowering the melt δ^{18}O. The resulting evolved melts are extracted once ∼55–65% crystallinity is reached. The extracted silicic melts ascend and then undergo minor additional cooling and crystallization at shallower levels, where they may mix with other silicic segregations and/or partially remobilize and assimilate older silicic intrusions before either erupting or solidifying. The crystal cargoes of the erupted rhyolites predominantly reflect these later processes occurring after melt extraction, and we infer that most crystals derived from more mafic melts are left behind in the mush and ultimately form cumulates at depth.

Our multi-stage model for the origin of Krafla rhyolites bears similarities to the two-step model recently proposed by Hampton *et al.* (2021). In their model, assimilation and fractional crystallization produces a low-δ^{18}O mafic to intermediate melt, which then ascends and undergoes further differentiation by fractional crystallization, accompanied by little to no further assimilation of low-δ^{18}O altered crust, to reach rhyolitic compositions. We suggest that the early stage of AFC envisaged by Hampton *et al.* (2021) is equivalent to the stage of mush formation envisaged here, and that their second stage reflects the shallow differentiation and mixing of extracted silicic melts (plus probable recycling of felsic intrusives) recorded by most macrocrysts.

An outstanding issue in understanding the origin of Krafla rhyolites is the clear compositional gap ('Daly gap') in erupted compositions between ∼57 and 71 wt% SiO_2, excluding hybrid magmas formed by basalt-rhyolite mixing (Jónasson, 1994). This dearth of intermediate compositions has previously been used as evidence against generation of Icelandic rhyolites by AFC from basaltic parents (Jónasson, 1994, 2007), based on the assumption that continuous, near-liquidus differentiation along a liquid line of descent should produce

intermediate magmas that also erupt. However, it is now recognized in many settings worldwide that such compositional gaps do not necessarily reflect a paucity of intermediate compositions at depth (e.g. Natali *et al.*, 2011; Barker *et al.*, 2013; Szymanowski *et al.*, 2015). Indeed, Dufek & Bachmann (2010) argue that such gaps may be an inherent feature of crystal fractionation and crystal mush formation, with the preferential extraction of melts in the ~50–70% crystallinity window favouring the eruption of highly fractionated silicic interstitial melts over intermediate ones formed earlier on the liquid line of descent. Interestingly, the lower bound on this optimal crystallinity window corresponds with liquid compositions of ~65–72 wt% SiO_2 in our MELTS models (Fig. 15), coinciding well with the upper (~71 wt% SiO_2) compositional limit of the Daly gap at Krafla (Jónasson, 1994). We thus suggest that this Daly gap does not reflect a paucity of intermediate melts at depth, but rather the preferential extraction and eruption of more evolved melts at later stages of magmatic differentiation.

The bulk fractionated solid composition predicted by our MELTS models after 50–70% crystallization is invariably mafic. Extensive crystallization of evolved quartz tholeiite basalts, followed by efficient extraction of the resultant silicic interstitial melt, would thus leave behind a mafic cumulate residue dominated by plagioclase, pyroxene, and Fe-Ti oxides (Fig. 15). The process of mush formation from evolved basaltic melts followed by melt extraction may thus explain the compositional bimodality of intrusive rocks in the exhumed cores of some Tertiary central volcanoes, as well as in erupted products at on-rift central volcanoes such as Krafla.

SUMMARY AND CONCLUSIONS

1. Crystals in the Krafla rhyolites comprise a mix of true phenocrysts native to their host magma and grains with antecrystic interiors derived from compositionally similar silicic magmas or felsic intrusives. Scarce cores derived from mafic wallrock or restite also occur. Crystal zoning patterns reflect diverse and complex magmatic histories superimposed on a dominant trend of progressive cooling and differentiation.

2. Late-stage storage and differentiation of Krafla rhyolites occurs largely in isolation from the underlying mafic system. Most crystals did not experience mafic recharge events during crystal growth.

3. Melting experiments on altered basalts and metabasalts support recent isotopic and modelling arguments against a partial melting origin for Krafla rhyolites (Hampton *et al.*, 2021). Low degrees of melting (~10% by mass) across a narrow temperature interval (<~50°C) are required to produce melts resembling the Krafla rhyolites purely by partial melting of altered basalts. Extracting volumes of partial melt sufficient to match the largest rhyolitic eruptions at Krafla requires this narrow

temperature window to be maintained across an unreasonably large volume of crust and is therefore untenable.

4. Shallow AFC of the evolved quartz tholeiite basalts typical of the central volcano can produce silicic melts with similar major and trace element chemistries to the Krafla rhyolites. MELTS fractional crystallization or AFC models predict liquid compositions resembling the observed rhyolitic compositions within the ~50–70 vol% crystallinity window at which extraction of interstitial melts from crystal mushes is most efficient. We thus propose that low-$\delta^{18}O$ silicic melts at Krafla are extracted from mush bodies formed by AFC in the shallow crust. These melts are extracted and undergo subsequent secondary processing at shallower depths, where they mix with other silicic magma batches and/or remobilize and assimilate shallow silicic mush or intrusions.

5. The Daly gap at Krafla does not reflect a paucity of intermediate melts at depth, but rather the preferential extraction and eruption of more evolved melts at later stages of magmatic differentiation. Efficient extraction of silicic melts from quartz tholeiite mushes in the ~50–70% crystallinity window leaves a mafic residue, which may explain the paucity of intermediate intrusive rocks in the exposed plutonic cores of some Tertiary Icelandic central volcanoes as well as the compositional gaps observed in erupted products of Krafla and other on-rift central volcanoes in Iceland.

SUPPLEMENTARY DATA

Supplementary data are available at *Journal of Petrology* online.

REFERENCES

Agustsdottir, T., Gudmundsson, M. T. & Einarsson, P. (2010). A gravity study of silicic domes in the Krafla area. *N-Iceland. Jökull* **60**, 135–148.

Almeev, R. R., Bolte, T., Nash, B. P., Holtz, F., Erdmann, M. & Cathey, H. E. (2012). High-temperature, low-H_2O silicic magmas of the Yellowstone hotspot: an experimental study of rhyolite from the Bruneau–Jarbidge eruptive center, central Snake River Plain, USA. *Journal of Petrology* **53**, 1837–1866.

Ármannsson, H., Guðmundsson, Á. & Steingrímsson, B. S. (1987). Exploration and development of the Krafla geothermal area. *Jökull* **37**, 13–30.

Árnason, K. (2020). New conceptual model for the magma-hydrothermal-tectonic system of Krafla, NE Iceland. *Geosciences* **10**, 34.

Astbury, R. L., Petrelli, M., Ubide, T., Stock, M. J., Arienzo, I., D'Antonio, M. & Perugini, D. (2018). Tracking plumbing system dynamics at the Campi Flegrei caldera, Italy: high-resolution trace element mapping of the Astroni crystal cargo. *Lithos* **318–319**, 464–477.

Bachmann, O. & Bergantz, G. W. (2004). On the origin of crystal-poor rhyolites: extracted from batholithic crystal mushes. *Journal of Petrology* **45**, 1565–1582.

Banik, T. J., Miller, C. F., Fisher, C. M., Coble, M. A. & Vervoort, J. D. (2018). Magmatic-tectonic control on the generation of silicic magmas in Iceland: constraints from Hafnarfjall-Skarðsheiði volcano. *Lithos* **318–319**, 326–339.

Barker, S. J., Wilson, C. J. N., Baker, J. A., Millet, M.-A., Rotella, M. D., Wright, I. C. & Wysoczanski, R. J. (2013). Geochemistry and petrogenesis of silicic magmas in the intra-oceanic Kermadec Arc. *Journal of Petrology* **54**, 351–391.

Beard, J. S. & Lofgren, G. E. (1989). Effect of water on the composition of partial melts of greenstone and amphibolite. *Science* **244**, 195–197.

Beard, J. S. & Lofgren, G. E. (1991). Dehydration melting and water-saturated melting of basaltic and andesitic greenstones and amphibolites at 1, 3, and 6. 9 kb. *Journal of Petrology* **32**, 365–401.

Bergþórsdóttir, I. A. (2018). The role of apatite in Hekla magmas: trace element partitioning between minerals and melt. Unpublished M.S. thesis, University of Iceland, p. 113.

Bindeman, I., Gurenko, A., Carley, T., Miller, C., Martin, E. & Sigmarsson, O. (2012). Silicic magma petrogenesis in Iceland by remelting of hydrothermally altered crust based on oxygen isotope diversity and disequilibria between zircon and magma with implications for MORB. *Terra Nova* **24**, 227–232.

Blundy, J. & Wood, B. (1994). Prediction of crystal–melt partition coefficients from elastic moduli. *Nature* **372**, 452–454.

Bolte, T., Holtz, F., Almeev, R. & Nash, B. (2015). The Blacktail Creek Tuff: an analytical and experimental study of rhyolites from the Heise volcanic field, Yellowstone hotspot system. *Contributions to Mineralogy and Petrology* **169**, 15.

Brugman, K. K. & Till, C. B. (2019). A low-aluminum clinopyroxene-liquid geothermometer for high-silica magmatic systems. *American Mineralogist* **104**, 996–1004.

Bunsen, R. (1851). Ueber die processe der vulkanischen gesterins-bildungen Islands (On the process of volcanic rock formation in Iceland). *Annalen der Physik und Chemie* **159**, 197–272.

Calderone, G. M., Grönvold, K. & Oskarsson, N. (1990). The welded air-fall tuff layer at Krafla, northern Iceland: a composite eruption triggered by injection of basaltic magma. *Journal of Volcanology and Geothermal Research* **44**, 303–314.

Carley, T. L., Miller, C. F., Fisher, C. M., Hanchar, J. M., Vervoort, J. D., Schmitt, A. K., Economos, R. C., Jordan, B. T., Padilla, A. J. & Banik, T. J. (2020). Petrogenesis of silicic magmas in Iceland through space and time: the isotopic record preserved in zircon and whole rocks. *The Journal of Geology* **128**, 1–28.

Carley, T. L., Miller, C. F., Wooden, J. L., Bindeman, I. N. & Barth, A. P. (2011). Zircon from historic eruptions in Iceland: reconstructing storage and evolution of silicic magmas. *Mineralogy and Petrology* **102**, 135–161.

Carley, T. L., Miller, C. F., Wooden, J. L., Padilla, A. J., Schmitt, A. K., Economos, R. C., Bindeman, I. N. & Jordan, B. T. (2014). Iceland is not a magmatic analog for the Hadean: evidence from the zircon record. *Earth and Planetary Science Letters* **405**, 85–97.

Carmichael, I. S. E. (1964). The petrology of Thingmuli, a Tertiary volcano in eastern Iceland. *Journal of Petrology* **5**, 435–460.

Carmichael, I. S. E. (1967). The iron-titanium oxides of salic volcanic rocks and their associated ferromagnesian silicates. *Contributions to Mineralogy and Petrology* **14**, 36–64.

Castro, J. M., Schipper, C. I., Mueller, S. P., Militzer, A. S., Amigo, A., Parejas, C. S. & Jacob, D. (2013). Storage and eruption of near-liquidus rhyolite magma at Cordón Caulle, Chile. *Bulletin of Volcanology* **75**, 1–17.

Charreteur, G., Tegner, C. & Haase, K. (2013). Multiple ways of producing intermediate and silicic rocks within Thingmúli and other Icelandic volcanoes. *Contributions to Mineralogy and Petrology* **166**, 471–490.

Condomines, M., Grönvold, K., Hooker, P. J., Muehlenbachs, K., O'Nions, R. K., Óskarsson, N. & Oxburgh, E. R. (1983). Helium, oxygen, strontium and neodymium isotopic relationships in Icelandic volcanics. *Earth and Planetary Science Letters* **66**, 125–136.

Cooper, K. M. (2017). What does a magma reservoir look like? The "crystal's-eye" view. *Elements* **13**, 23–28.

Cooper, K. M., Sims, K. W. W., Eiler, J. M. & Banerjee, N. (2016). Timescales of storage and recycling of crystal mush at Krafla Volcano, Iceland. *Contributions to Mineralogy and Petrology* **171**, 1–19.

Couch, S., Sparks, R. S. J. & Carroll, M. R. (2001). Mineral disequilibrium in lavas explained by convective self-mixing in open magma chambers. *Nature* **411**, 1037–1039.

Dufek, J. & Bachmann, O. (2010). Quantum magmatism: magmatic compositional gaps generated by melt-crystal dynamics. *Geology* **38**, 687–690.

Eiler, J. M. (2001). Oxygen Isotope variations of basaltic Lavas and upper mantle rocks. *Reviews in Mineralogy and Geochemistry* **43**, 319–364.

Eichelberger, J. (2020). Distribution and transport of thermal energy within magma–hydrothermal systems. *Geosciences* **10**, 212.

Eichelberger, J. C. (2019). Planning an international magma observatory. *Eos* **100**. https://eos.org/science-updates/planning-an-international-magma-observatory.

Einarsson, P. (1978). S-wave shadows in the Krafla Caldera in NE-Iceland, evidence for a magma chamber in the crust. *Bulletin Volcanologique* **41**, 187–195.

Elders, W. A., Friðleifsson, G. O., Zierenberg, R. A., Pope, E. C., Mortensen, A. K., Gudmundsson, A., Lowenstern, J. B., Marks, N. E., Owens, L., Bird, D. K., Reed, M., Olsen, N. J. & Schiffman, P. (2011). Origin of a rhyolite that intruded a geothermal well while drilling at the Krafla volcano. *Geology* **39**, 231–234.

Erdmann, M., Fischer, L. A., France, L., Zhang, C., Godard, M. & Koepke, J. & (2015). Anatexis at the roof of an oceanic magma chamber at IODP Site 1256 (equatorial Pacific): an experimental study. *Contributions to Mineralogy and Petrology* **169**, 39.

Fowler, S. J. & Spera, F. J. (2010). A metamodel for crustal magmatism: phase equilibria of giant ignimbrites. *Journal of Petrology* **51**, 1783–1830.

France, L., Koepke, J., Ildefonse, B., Cichy, S. B. & Deschamps, F. (2010). Hydrous partial melting in the sheeted dike complex at fast spreading ridges: experimental and natural observations. *Contributions to Mineralogy and Petrology* **160**, 683–704.

Fujimaki, H. (1986). Partition coefficients of Hf, Zr, and REE between zircon, apatite, and liquid. *Contributions to Mineralogy and Petrology* **94**, 42–45.

Furman, T., Frey, F. A. & Meyer, P. S. (1992). Petrogenesis of evolved basalts and rhyolites at Austurhorn, southeastern Iceland: the role of fractional crystallization. *Journal of Petrology* **33**, 1405–1445.

Gardner, J. E., Befus, K. S., Gualda, G. A. R. & Ghiorso, M. S. (2014). Experimental constraints on rhyolite-MELTS and the Late Bishop Tuff magma body. *Contributions to Mineralogy and Petrology* **168**, 1051.

Geist, D., Harpp, K., Oswald, P., Wallace, P., Bindeman, I. & Christensen, B. (2021). Hekla revisited: fractionation of a magma body at historical timescales. *Journal of Petrology*, in Press.

Gelman, S. E., Deering, C. D., Bachmann, O., Huber, C. & Gutiérrez, F. J. (2014). Identifying the crystal graveyards remaining after large silicic eruptions. *Earth and Planetary Science Letters* **403**, 299–306.

Ghiorso, M. S. & Sack, R. O. (1995). Chemical mass transfer in magmatic processes IV. A revised and internally consistent thermodynamic model for the interpolation and extrapolation of liquid-solid equilibria in magmatic systems at elevated temperatures and pressures. *Contributions to Mineralogy and Petrology* **119**, 197–212.

Ginibre, C., Kronz, A. & Wörner, G. (2002a). High-resolution quantitative imaging of plagioclase composition using accumulated backscattered electron images: new constraints on oscillatory zoning. *Contributions to Mineralogy and Petrology* **142**, 436–448.

Ginibre, C., Wörner, G. & Kronz, A. (2002b). Minor- and trace-element zoning in plagioclase: implications for magma chamber processes at Parinacota volcano, northern Chile. *Contributions to Mineralogy and Petrology* **143**, 300–315.

Ginibre, C., Worner, G. & Kronz, A. (2007). Crystal zoning as an archive for magma evolution. *Elements* **3**, 261–266.

Gleeson, M. L. M., Stock, M. J., Pyle, D. M., Mather, T. A., Hutchison, W., Yirgu, G. & Wade, J. (2017). Constraining magma storage conditions at a restless volcano in the Main Ethiopian Rift using phase equilibria models. *Journal of Volcanology and Geothermal Research* **337**, 44–61.

Grönvold, K. (1984). Myvatn fires 1724-1729: Chemical composition of the lava. In: Nordic Volcanological Institute Report **8401**, 30.

Grönvold, K. & Mäkipää, H. (1978). Chemical composition of Krafla lavas 1975-1977. In: Nordic Volcanological Institute Report **7816**, 49.

Guilbaud, M.-N., Blake, S., Thordarson, T. & Self, S. (2007). Role of syn-eruptive cooling and degassing on textures of lavas from the AD 1783–1784 Laki eruption, South Iceland. *Journal of Petrology* **48**, 1265–1294.

Gunnarsson, B., Marsh, B. D. & Taylor, H. P. (1998). Generation of Icelandic rhyolites: silicic lavas from the Torfajökull central volcano. *Journal of Volcanology and Geothermal Research* **83**, 1–45.

Gurenko, A. A., Bindeman, I. N. & Sigurdsson, I. A. (2015). To the origin of Icelandic rhyolites: insights from partially melted leucocratic xenoliths. *Contributions to Mineralogy and Petrology* **169**, 49.

Haggerty, S. E. (1991). Oxide textures; a mini-atlas. *Reviews in Mineralogy and Geochemistry* **25**, 129–219.

Halldórsson, S. A., Bali, E., Hartley, M. E., Neave, D. A., Peate, D. W., Guðfinnsson, G. H., Bindeman, I., Whitehouse, M. J., Riishuus, M. S., Pedersen, G. B. M., Jakobsson, S., Askew, R., Gallagher, C. R., Guðmundsdóttir, E. R., Gudnason, J., Moreland, W. M., Óskarsson, B. V., Nikkola, P., Reynolds, H. I., Schmith, J. & Thordarson, T. (2018). Petrology and geochemistry of the 2014–2015 Holuhraun eruption, central Iceland: compositional and mineralogical characteristics, temporal variability and magma storage. *Contributions to Mineralogy and Petrology* **173**, 64.

Hattori, K. & Muehlenbachs, K. (1982). Oxygen isotope ratios of the Icelandic crust. *Journal of Geophysical Research: Solid Earth* **87**, 6559–6565.

Hampton, R. L., Bindeman, I. N., Stern, R. A., Coble, M. A. & Rooyakkers, S. M. (2021). A microanalytical oxygen isotopic and U-Th geochronologic investigation of rhyolite petrogenesis at the Krafla central volcano, Iceland. *Journal of Volcanology and Geothermal Research* **414**, 107229.

Hards, V. L., Kempton, P. D., Thompson, R. N. & Greenwood, P. B. (2000). The magmatic evolution of the Snæfell volcanic centre; an example of volcanism during incipient rifting in Iceland. *Journal of Volcanology and Geothermal Research* **99**, 97–121.

Hartley, M. E., Shorttle, O., Maclennan, J., Moussallam, Y. & Edmonds, M. (2017). Olivine-hosted melt inclusions as an archive of redox heterogeneity in magmatic systems. *Earth and Planetary Science Letters* **479**, 192–205.

Hattori, K. & Muehlenbachs, K. (1982). Oxygen isotope ratios of the Icelandic crust. *Journal of Geophysical Research: Solid Earth* **87**, 6559–6565.

Hemond, C., Arndt, N. T., Lichtenstein, U., Hofmann, A. W., Oskarsson, N. & Steinthorsson, S. (1993). The heterogeneous Iceland plume: Nd-Sr-O isotopes and trace element constraints. *Journal of Geophysical Research* **98**, 15833–15850.

Hildreth, W. (2004). Volcanological perspectives on Long Valley, Mammoth Mountain, and Mono Craters: several contiguous but discrete systems. *Journal of Volcanology and Geothermal Research* **136**, 169–198.

Hjartardóttir, Á. R., Einarsson, P., Bramham, E. & Wright, T. J. (2012). The Krafla fissure swarm, Iceland, and its formation by rifting events. *Bulletin of Volcanology* **74**, 2139–2153.

Hjartardóttir, Á. R., Einarsson, P., Gudmundsson, M. T. & Högnadóttir, T. (2016). Fracture movements and graben subsidence during the 2014 Bárðarbunga dike intrusion in Iceland. *Journal of Volcanology and Geothermal Research* **310**, 242–252.

Hollingsworth, J., Leprince, S., Ayoub, F. & Avouac, J.-P. (2012). Deformation during the 1975–1984 Krafla rifting crisis, NE Iceland, measured from historical optical imagery. *Journal of Geophysical Research: Solid Earth* **117**, 1–24.

Holtz, F., Johannes, W., Tamic, N. & Behrens, H. (2001). Maximum and minimum water contents of granitic melts generated in the crust: a reevaluation and implications. *Lithos* **56**, 1–14.

Huang, F., Scaillet, B., Wang, R., Erdmann, S., Chen, Y., Faure, M., Liu, H., Xie, L., Wang, B. & Zhu, J. (2019). Experimental constraints on intensive crystallization parameters and fractionation in A-type granites: a case study on the Qitianling pluton, South China. *Journal of Geophysical Research: Solid Earth* **124**, 10132–10152.

Humphreys, M. C. S., Blundy, J. D. & Sparks, R. S. J. (2006). Magma evolution and open-system processes at Shiveluch Volcano: insights from phenocryst zoning. *Journal of Petrology* **47**, 2303–2334.

Jerram, D. A., Dobson, K. J., Morgan, D. J. & Pankhurst, P. J. (2018). The petrogenesis of magmatic systems: using

igneous textures to understand magmatic processes. In: Burchardt, S. (ed.) *Volcanic and Igneous Plumbing Systems*. Amsterdam: Elsevier, 191–229.

Jónasson, K. (1994). Rhyolite volcanism in the Krafla central volcano, north-east Iceland. *Bulletin of Volcanology* **56**, 516–528.

Jónasson, K. (2007). Silicic volcanism in Iceland: composition and distribution within the active volcanic zones. *Journal of Geodynamics* **43**, 101–117.

Kennedy, B. M., Holohan, E. P., Stix, J., Gravley, D. M., Davidson, J. R. J. & Cole, J. W. (2018). Magma plumbing beneath collapse caldera volcanic systems. *Earth-Science Reviews* **177**, 404–424.

Klimm, K., Holtz, F., Johannes, W. & King, P. L. (2003). Fractionation of metaluminous A-type granites: an experimental study of the Wangrah Suite, Lachlan Fold Belt, Australia. *Precambrian Research* **124**, 327–341.

Klimm, K., Holtz, F. & King, P. L. (2008). Fractionation vs. magma mixing in the Wangrah Suite A-type granites, Lachlan Fold Belt. *Lithos* **102**, 415–434.

Koepke, J., Feig, S. T., Snow, J. & Freise, M. (2004). Petrogenesis of oceanic plagiogranites by partial melting of gabbros: an experimental study. *Contributions to Mineralogy and Petrology* **146**, 414–432.

Kress, V. C. & Carmichael, I. S. E. (1991). The compressibility of silicate liquids containing Fe_2O_3 and the effect of composition, temperature, oxygen fugacity and pressure on their redox states. *Contributions to Mineralogy and Petrology* **108**, 82–92.

Lucic, G., Berg, A.-S. & Stix, J. (2016). Water-rich and volatile-undersaturated magmas at Hekla volcano. *Geochemistry, Geophysics, Geosystems* **17**, 3111–3130.

Lundgaard, K. L. & Tegner, C. (2004). Partitioning of ferric and ferrous iron between plagioclase and silicate melt. *Contributions to Mineralogy and Petrology* **147**, 470–483.

Macdonald, R., McGarvie, D. W., Pinkerton, H., Smith, R. L. & Palacz, A. (1990). Petrogenetic evolution of the Torfajökull volcanic complex, Iceland I. Relationship between the magma types. *Journal of Petrology* **31**, 429–459.

Macdonald, R., Sparks, R. S. J., Sigurdsson, H., Mattey, D. P., McGarvie, D. W. & Smith, R. L. (1987). The 1875 eruption of Askja volcano, Iceland: combined fractional crystallization and selective contamination in the generation of rhyolitic magma. *Mineralogical Magazine* **51**, 183–202.

Marsh, B. D., Gunnarsson, B., Congdon, R. & Carmody, R. (1991). Hawaiian basalt and Icelandic rhyolite: indicators of differentiation and partial melting. *Geologische Rundschau* **80**, 481–510.

Martin, E., Martin, H. & Sigmarsson, O. (2008). Could Iceland be a modern analogue for the Earth's early continental crust? *Terra Nova* **20**, 463–468.

Martin, E. & Sigmarsson, O. (2007). Crustal thermal state and origin of silicic magma in Iceland: the case of Torfajökull, Ljósufjöll and Snæfellsjökull volcanoes. *Contributions to Mineralogy and Petrology* **153**, 593–605.

Martin, E. & Sigmarsson, O. (2010). Thirteen million years of silicic magma production in Iceland: links between petrogenesis and tectonic settings. *Lithos* **116**, 129–144.

Masotta, M., Mollo, S., Nazzari, M., Tecchiato, V., Scarlato, P., Papale, P. & Bachmann, O. (2018). Crystallization and partial melting of rhyolite and felsite rocks at Krafla volcano: a comparative approach based on mineral and glass chemistry of natural and experimental products. *Chemical Geology* **483**, 603–618.

McDonough, W. F. & Sun, S-S. (1995). The composition of the Earth. *Chemical Geology* **120**, 223–253.

McGarvie, D. (2009). Rhyolitic volcano–ice interactions in Iceland. *Journal of Volcanology and Geothermal Research* **185**, 367–389.

McGarvie, D. W., Macdonald, R., Pinkerton, H. & Smith, R. L. (1990). Petrogenetic evolution of the Torfajökull volcanic complex, Iceland II. The role of magma mixing. *Journal of Petrology* **31**, 461–481.

Mortensen, A. K., Grönvold, K., Guðmundsson, Á., Steingrímsson, B. & Egilson, T. (2010). Quenched silicic glass from Well KJ-39 in Krafla, North-Eastern Iceland. In: *Proceedings of the World Geothermal Congress*, Bali, Indonesia, April 25–29, 2010, paper 1284.

Natali, C., Beccaluva, L., Bianchini, G. & Siena, F. (2011). Rhyolites associated to Ethiopian CFB: clues for initial rifting at the Afar plume axis. *Earth and Planetary Science Letters* **312**, 59–68.

Nichols, A. R. L., Carroll, M. R. & Höskuldsson, Á. (2002). Is the Iceland hot spot also wet? Evidence from the water contents of undegassed submarine and subglacial pillow basalts. *Earth and Planetary Science Letters* **202**, 77–87.

Nicholson, H. (1990). The magmatic evolution of Krafla, NE Iceland. Unpublished Ph.D. thesis, University of Edinburgh, p. 286.

Nicholson, H., Condomines, M., Fitton, J. G., Fallick, A. E., Grönvold, K. & Rogers, G. (1991). Geochemical and isotopic evidence for crustal assimilation beneath Krafla, Iceland. *Journal of Petrology* **32**, 1005–1020.

O'Nions, R. K. & Grönvold, K. (1973). Petrogenetic relationships of acid and basic rocks in Iceland: Sr-isotopes and rare-earth elements in late and postglacial volcanics. *Earth and Planetary Science Letters* **19**, 397–409.

Óskarsson, N., Sigvaldason, G. E. & Steinthórsson, S. (1982). A dynamic model of rift zone petrogenesis and the regional petrology of Iceland. *Journal of Petrology* **23**, 28–74.

Óskarsson, N., Steinthorsson, S. & Sigvaldason, G. E. (1985). Iceland geochemical anomaly: origin, volcanotectonics, chemical fractionation and isotope evolution of the crust. *Journal of Geophysical Research* **90**, 10011–10025.

Owen, J., Tuffen, H. & McGarvie, D. W. (2013a). Explosive subglacial rhyolitic eruptions in Iceland are fuelled by high magmatic H_2O and closed-system degassing. *Geology* **41**, 251–254.

Owen, J., Tuffen, H. & McGarvie, D. W. (2013b). Pre-eruptive volatile content, degassing paths and depressurisation explaining the transition in style at the subglacial rhyolitic eruption of Dalakvísl, South Iceland. *Journal of Volcanology and Geothermal Research* **258**, 143–162.

Pope, E. C., Bird, D. K. & Arnórsson, S. (2013). Evolution of low-^{18}O Icelandic crust. *Earth and Planetary Science Letters* **374**, 47–59.

Portnyagin, M., Hoernle, K., Storm, S., Mironov, N., van den Bogaard, C. & Botcharnikov, R. (2012). H_2O-rich melt inclusions in fayalitic olivine from Hekla volcano: implications for phase relationships in silicic systems and driving forces of explosive volcanism on Iceland. *Earth and Planetary Science Letters* **357–358**, 337–346.

Putirka, K. D. (2008). Thermometers and barometers for volcanic systems. *Reviews in Mineralogy and Geochemistry* **69**, 61–120.

Rooyakkers, S. M. (2020). New insights on rhyolitic and mixed rhyolitic-basaltic magmatism and volcanism at Krafla central volcano, Iceland. Unpublished Ph.D. thesis, McGill University, p. 26.

Rooyakkers, S. M., Stix, J., Berlo, K. & Barker, S. J. (2020). Emplacement of unusual rhyolitic to basaltic ignimbrites during collapse of a basalt-dominated caldera: the Halarauður eruption. *GSA Bulletin* **132**, 1881–1902.

Rooyakkers, S. M., Stix, J., Berlo, K., Petrelli, M. & Sigmundsson, F. (2021). Eruption risks from covert silicic magma bodies. *Geology* **49**, 921–925.

Ruprecht, P. & Wörner, G. (2007). Variable regimes in magma systems documented in plagioclase zoning patterns: El Misti

stratovolcano and Andahua monogenetic cones. *Journal of Volcanology and Geothermal Research* **165**, 142–162.

Saubin, E., Kennedy, B., Tuffen, H., Nichols, A. R. L., Villeneuve, M., Bindeman, I., Mortensen, A., Schipper, C. I., Wadsworth, F. B., Watson, T. & Zierenberg, R. (2021). Textural and geochemical window into the IDDP-1 rhyolitic melt, Krafla, Iceland, and its reaction to drilling. *Geological Society of America Bulletin*.

Sæmundsson, K. (1979). Outline of the geology of Iceland. *Jökull* **29**, 7–27.

Sæmundsson, K. (1991). Jarðfræði Kröflukerfisins (Geology of the Krafla Volcanic System). In: Garðarson, A. & Einarsson, Á. (eds), *Náttúra Mývatns (Mývatn's Nature). Reykjavík: Hid Íslenska Náttúrufræðifélag.* 24–95.

Sæmundsson, K., Hjartarson, Á., Kaldal, I., Sigurgeirsson, M. A., Kristinsson, S. G. & Vikingsson, S. (2012). *Geological Map of the Northern Volcanic Zone, Iceland, Northern Part.* Iceland Geosurvey and Landsvirkjun, scale 1:100,000.

Sæmundsson, K. & Pringle, M. S. (2000). Um aldur berglaga Í Kröflukerfinu (On the age of rock strata in the Krafla system). In: *Proceedings of the Geoscience Society of Iceland Spring Meeting Abstracts, Reykjavík*, 26–27.

Scaillet, B. & Macdonald, R. (2003). Experimental constraints on the relationships between peralkaline rhyolites of the Kenya Rift Valley. *Journal of Petrology* **44**, 1867–1894.

Schattel, N., Portnyagin, M., Golowin, R., Hoernle, K. & Bindeman, I. (2014). Contrasting conditions of rift and off-rift silicic magma origin on Iceland. *Geophysical Research Letters* **41**, 5813–5820.

Schiffman, P., Zierenberg, R. A., Mortensen, A. K., Friðleifsson, G. Ó. & Elders, W. A. (2014). High temperature metamorphism in the conductive boundary layer adjacent to a rhyolite intrusion in the Krafla geothermal system. *Geothermics* **49**, 42–48.

Selbekk, R. S. & Trønnes, R. G. (2007). The 1362 AD Öræfajökull eruption, Iceland: petrology and geochemistry of large-volume homogeneous rhyolite. *Journal of Volcanology and Geothermal Research* **160**, 42–58.

Shorttle, O., Moussallam, Y., Hartley, M. E., Maclennan, J., Edmonds, M. & Murton, B. J. (2015). Fe-XANES analyses of Reykjanes Ridge basalts: implications for oceanic crust's role in the solid Earth oxygen cycle. *Earth and Planetary Science Letters* **427**, 272–285.

Sigmarsson, O., Condomines, M. & Fourcade, S. (1992). A detailed Th, Sr and O isotope study of Hekla: differentiation processes in an Icelandic Volcano. *Contributions to Mineralogy and Petrology* **112**, 20–34.

Sigmarsson, O., Hémond, C., Condomines, M., Fourcade, S. & Oskarsson, N. (1991). Origin of silicic magma in Iceland revealed by Th isotopes. *Geology* **19**, 621–624.

Sigurdsson, H. (1968). Petrology of acid xenoliths from Surtsey. *Geological Magazine* **105**, 440–453.

Sigurdsson, H. (1977). Generation of Icelandic rhyolites by melting of plagiogranites in the oceanic layer. *Nature* **269**, 25–28.

Sigurdsson, H. & Sparks, R. S. J. (1981). Petrology of rhyolitic and mixed magma ejecta from the 1875 Eruption of Askja, Iceland. *Journal of Petrology* **22**, 41–84.

Smith, P. M. & Asimow, P. D. (2005). Adiabat_1ph: a new public front-end to the MELTS, pMELTS, and pHMELTS models. *Geochemistry, Geophysics, Geosystems* **6**,

Spulber, S. D. & Rutherford, M. J. (1983). The origin of rhyolite and plagiogranite in oceanic crust: an experimental study. *Journal of Petrology* **24**, 1–25.

Stormer, J. C. (1983). The effects of recalculation on estimates of temperature and oxygen fugacity from analyses of multicomponent iron-titanium oxides. *American Mineralogist* **68**, 586–594.

Sun, S.-S. & McDonough, W. F. (1989). Chemical and isotopic systematics of oceanic basalts: implications for mantle composition and processes. In: Saunders, A. D. & Norry, M. J. (eds) *Implications for Mantle Composition and Processes, Magmatism in the Ocean Basins*. Geological Society, London, Special Publications **42**, 313–345.

Sverrisdottir, G. (2007). Hybrid magma generation preceding Plinian silicic eruptions at Hekla, Iceland: evidence from mineralogy and chemistry of two zoned deposits. *Geological Magazine* **144**, 643–659.

Szymanowski, D., Ellis, B. S., Bachmann, O., Guillong, M. & Phillips, W. M. (2015). Bridging basalts and rhyolites in the Yellowstone-Snake River Plain volcanic province: the elusive intermediate step. *Earth and Planetary Science Letters* **415**, 80–89.

Thorarinsson, S. (1979). The postglacial history of the Mývatn area. *Oikos* **32**, 16–28.

Thordarson, T. & Larsen, G. (2007). Volcanism in Iceland in historical time: volcano types, eruption styles and eruptive history. *Journal of Geodynamics* **43**, 118–152.

Thy, P., Beard, J. S. & Lofgren, G. E. (1990). Experimental constraints on the origin of Icelandic rhyolites. *The Journal of Geology* **98**, 417–421.

Toplis, M. J. & Carroll, M. R. (1995). An experimental study of the influence of oxygen fugacity on Fe-Ti oxide stability, phase relations, and mineral- melt equilibria ferro-basaltic systems. *Journal of Petrology* **36**, 1137–1170.

Troch, J., Ellis, B. S., Harris, C., Ulmer, P. & Bachmann, O. (2018). The effect of prior hydrothermal alteration on the melting behaviour during rhyolite formation in Yellowstone, and its importance in the generation of low-δ^{18}O magmas. *Earth and Planetary Science Letters* **481**, 338–349.

Tuffen, H. & Castro, J. M. (2009). The emplacement of an obsidian dyke through thin ice: Hrafntinnuhryggur, Krafla Iceland. *Journal of Volcanology and Geothermal Research* **185**, 352–366.

Ubide, T. & Kamber, B. S. (2018). Volcanic crystals as time capsules of eruption history. *Nature Communications* **9**, 326.

Walker, G. P. L. (1966). Acid volcanic rocks in Iceland. *Bulletin Volcanologique* **29**, 375–402.

Waters, L. E. & Lange, R. A. (2015). An updated calibration of the plagioclase-liquid hygrometer-thermometer applicable to basalts through rhyolites. *American Mineralogist* **100**, 2172–2184.

Weber, G. & Castro, J. M. (2017). Phase petrology reveals shallow magma storage prior to large explosive silicic eruptions at Hekla volcano. *Earth and Planetary Science Letters* **466**, 168–180.

Weisenberger, T. B., Axelsson, G., Arnaldsson, A., Blischke, A., Óskarsson, F., Ármannsson, H., Blanck, H., Helgadóttir, M., Berthet, J.-C C., Árnason, K., Ágústsson, K., Gylfadóttir, S. S. & Guðmundsdóttir, V. (2015). Revision of the conceptual model of the Krafla geothermal system. *Landsvirkjun Report* **LV-2015-040**.

White, W. M. (2013). *Geochemistry*. UK: Wiley-Blackwell.

Wood, B. J. & Blundy, J. D. (1997). A predictive model for rare earth element partitioning between clinopyroxene and anhydrous silicate melt. *Contributions to Mineralogy and Petrology* **129**, 166–181.

Zierenberg, R. A., Schiffman, P., Barfod, G. H., Lesher, C. E., Marks, N. E., Lowenstern, J. B., Mortensen, A. K., Pope, E. C., Bird, D. K., Reed, M. H., Friðleifsson, G. O. & Elders, W. A. (2013). Composition and origin of rhyolite melt intersected by drilling in the Krafla geothermal field, Iceland. *Contributions to Mineralogy and Petrology* **165**, 327–347.